

# Dynamic Estimation of Tea Flowering Based on an Improved YOLOv5 and ANN Model

## Authors

Qianxi Mi<sup>1,2</sup>, Pengcheng Yuan<sup>1,2</sup>, Chunlei Ma<sup>1,2</sup>, Jiedan Chen<sup>1,2\*</sup>, Mingzhe Yao<sup>1,2\*</sup>

## Affiliations

1 Key Laboratory of Biology, Genetics and Breeding of Special Economic Animals and Plants, Ministry of Agriculture and Rural Affairs, Tea Research Institute of the Chinese Academy of Agricultural Sciences, Hangzhou 310008, China.

2 National Key Laboratory for Tea Plant Germplasm Innovation and Resource Utilization, Tea Research Institute of the Chinese Academy of Agricultural Sciences, Hangzhou 310008, China.

\*Address correspondence to: Jiedan Chen (chenjd@tricaas.com); and Mingzhe Yao (yaomz@tricaas.com).

## Abstract

Tea flowers play a crucial role in taxonomic research and hybrid breeding for the tea plant. Tea flowering consumes the plant's nutrients, and flower thinning can regulate carbon-nitrogen metabolism, enhancing the yield and quality of young shoots. As traditional methods of observing tea flower traits are labor-intensive and inaccurate, we propose an effective framework for tea flowering quantifying. In this study, a highly representative and diverse dataset was constructed by collecting flower images from 29 tea accessions. Based on this dataset, the TflosYOLO model was built on the YOLOv5 architecture and enhanced with the Squeeze-and-Excitation (SE) network, which is the first model to offer a viable solution for detecting tea flowers and predicting flower quantities. The TflosYOLO model achieved an mAP50 of 0.874, outperforming YOLOv5, YOLOv7 and YOLOv8. Furthermore, this model was tested on 34 datasets encompassing 26 tea accessions, five flowering stages, various lighting conditions, and pruned/unpruned plants, demonstrating high generalization and robustness. The correlation coefficient ( $R^2$ ) between the predicted and actual flower counts was 0.974. Additionally, the TFSC (Tea Flowering Stage Classification) model - a novel Artificial Neural Network (ANN) was designed for automatic classification of the flowering stages. TFSC achieved an accuracy of 0.899. Dynamic analysis of flowering across 29 tea accessions in 2023 and 2024 was conducted, revealed significant variability in flower quantity and dynamics, with genetically similar accessions showing more consistent

flowering patterns. This framework provides a solution for quantifying tea flowering, and can serve as a reference for precision horticulture.

## 1. INTRODUCTION

Tea is one of the three major beverages in the world, and the tea plant is an important economic crop in multiple countries. With a cultivation history spanning thousands of years, China is home to a rich diversity of native tea accessions. In recent years, numerous distinct tea cultivars have been developed across various tea-growing regions, supporting the growth of the tea industry and promoting improvements in both quality and efficiency. As a perennial leaf crop, the economic value of tea plant primarily derives from its young shoots, and most research has focused on the growth and development of these shoots. However, as reproductive organs, tea flowers are crucial for conducting genetic and taxonomic studies. The flowering period is crucial for selecting parent plants for hybrid breeding, as it must be relatively synchronized for successful cross-breeding. Tea flowering consumes the plant nutrients so that flower thinning can regulate carbon-nitrogen metabolism, promoting vegetative growth while suppressing reproductive growth, further enhancing the yield of young shoots and increasing the amino acid content, which positively impacts tea quality[1,2]. Therefore, measuring the floral phenotypes of tea accessions is of great importance.

China has abundant phenotypic resources of tea plants, and significant differences exist between accessions in terms of flower quantity and flowering stage (including the onset and cessation of blooming, and the duration of the flowering stage). Tea flower quantity is a key trait of tea accessions, which is closely related to the genetic makeup of the accession, its growth status, cultivation practices, light conditions, and temperature. And the flowering stage of tea plants varies significantly depending on the planting region, genetic resources of the tea accession, and climatic differences across years. Breeding programs require investigations of flower quantity and flowering stages. However, Traditional methods for observing tea flower traits, such as manual measurements and naked eyed observation, are labor-intensive and prone to inaccuracies. For example, the "fixed-plant removal method" involves selecting 1-5 representative tea plants, removing flowers, and counting them, then estimating overall flower quantity and yield. This method has limited representativeness for the entire accession. Moreover, removing flowers can impact flowering rates. Another common method is flower quantity grading, where flowers are estimated and categorized manually, it typically conducted only once or twice, which is insufficient given the long flowering periods of tea plants and the significant variation in flowering time across different accessions. Additionally, given the diversity of tea accessions, with differences in flower size, color, quantity,

and flowering period, previous studies have only selected a small number of accessions[1], making it difficult to accurately describe the regional characteristics of the species. Therefore, there is a clear need to develop efficient, precise, and highly generalized phenotyping technologies for tea flowers.

In recent years, advancements in machine learning, deep learning, computer vision technologies, and drones have significantly impacted agricultural applications, such as yield prediction, crop growth monitoring, automated harvesting, and quality detection. Traditional machine learning methods (ML), including support vector machines (SVM), random forests, partial least squares regression (PLSR), K-means clustering, and artificial neural networks (ANN), take a data-driven approach to model the relationships between input data and labels, such as crop yield[3]. These machine learning systems are capable of processing large datasets and handling non-linear tasks efficiently[4]. For example, A machine learning algorithm incorporating K-means clustering was developed for grapevine inflorescence detection, classification, and flower number estimation, which demonstrates high accuracy[5]. In another study, six different machine learning algorithms, including ridge regression, SVM, random forest, Gaussian process, K-means, and Cubist was utilized by Song et al.[6] to establish yield prediction models, based on drone-collected visible and multispectral images of wheat canopies during the grain filling stage. As for machine learning in tea research, Tu et al.[7] utilized UAV-acquired hyperspectral data to build a classification model for tea accessions and estimate the content of key chemicals related to tea flavor. Their research indicated that SVM and ANN models were most effective for tea plant classification, while PLSR showed the highest accuracy in predicting biochemical parameters. Chen et al.[8] compared the performance of multilayer perceptron (MLP), SVM, random forests (RF), and PLSR using hyperspectral data from tea plants, developing Tea-DTC model for evaluating drought resistance traits in 10 tea plant germplasm resources.

However, traditional machine learning methods are heavily reliant on manually selected features under controlled conditions, and their robustness tends to be limited, particularly in complex field environments. These methods often struggle to handle the challenges posed by the dynamic and variable real-world agricultural environments[9,10]. Deep learning (DL) methods, on the other hand, excel in discovering patterns and hidden information from large datasets using neural networks[11]. Unlike traditional machine learning, DL approaches are better suited for complex scenarios and require large amounts of data for training. Recent deep learning algorithms, such as Faster R-CNN, ResNet, and YOLO-based models, have demonstrated superior performance in crop yield estimation[12,13], growth monitoring[14,15], and object detection for fruits and other crop targets[16–18]. YOLOv5, developed by Glenn Jocher et al.[19], is an improved version of YOLOv3.

It is characterized by a relatively small model size and fast processing speed, making it suitable for mobile deployment. In recent years, YOLO-based algorithms, particularly YOLOv5 have been widely applied to object detection in agriculture, demonstrating superior performance on agricultural datasets[20]. Additionally, the integration of machine learning, deep learning, and plant phenotyping platforms, along with UAV technology, has resulted in the development of many new and efficient techniques. For instance, RGB and multispectral images was utilized to identify the tasseling stage of maize[21]. Drone time-series images and a Res2Net50 model was used to identify five growth stages of rice germplasm using, achieving good prediction results for the heading and flowering stages by combining RGB and multispectral images and developing a PLSR model[22]. Similarly, drone time-series images and deep learning models were applied for dynamic monitoring of maize ear area[23]. These advances have significantly contributed to the rapid and efficient extraction of plant information, facilitating accurate plant phenotyping.

Several automatic detection models for various flowers such as apple flowers, pear flowers, grapevine flowers, strawberry flowers and litchi flower, have been developed[5,10,24–28], as well as tea shoot detection models[29–33]. Notably, Wang et al.[34] used color thresholding followed by SVM classification to estimate mango inflorescence area, employing Faster R-CNN for panicle detection. Lin et al.[24] proposed a framework for counting flowers in Litchi panicles and quantifying male Litchi flowers, employing YOLACT++ for panicle segmentation and a novel algorithm based on density map regression, for accurate flower counting. The YOLOX was utilized by Xia et al.[10] for tree-level apple inflorescence detection, achieving the highest AP50 of 0.834 and AR50 of 0.933.

Despite the extensive research on object detection and growth monitoring models for other crops, the breadth of available data remains limited, particularly in relation to the diversity of crop accessions, which can significantly influence model performance and generalization. Thus, it is critical for models to exhibit high generalization capabilities, allowing them to be applied across different tea accessions for effective flower detection and flower quantity estimation. To date, however, no models have been specifically developed to detect tea plant flowers or observe tea flower phenotypes. To fill this gap, we propose a framework for tea flowering quantifying, comprising the TflosYOLO model and TFSC (Tea flowering stages classification) model. TflosYOLO model based on YOLOv5, is the first to offer a viable solution for detecting tea flowers and predicting flower quantities, with potential applications in tea flower thinning practices. TFSC model is a novel Artificial Neural Network (ANN) for Tea flowering stages classification. The framework is designed to enable dynamic monitoring of flower quantity and flowering periods

across various tea accessions, providing crucial support for tea plant breeding programs and phenotypic analysis of germplasm resources.

## 2. MATERIALS AND METHODS

### 2.1 Experimental Design

This study presents a framework for quantifying the tea flowering based on time-series images of tea flowers, deep learning, and machine learning. The framework (Fig. 1) consists of four key components: the TflosYOLO model, tea flower quantity, the TFSC model, and dynamic estimation and analysis of tea flowering. The process is outlined as follows: Mobile phone images of tea plant flowers are captured to establish a tea flower dataset, which is then used to train the TflosYOLO tea flower detection model. After the TflosYOLO model outputs the flower quantities, TFSC model is used to classify the flowering stages. Based on the above components, dynamic estimation and analysis of tea flowering are conducted. The detailed methodology is presented in the following section.

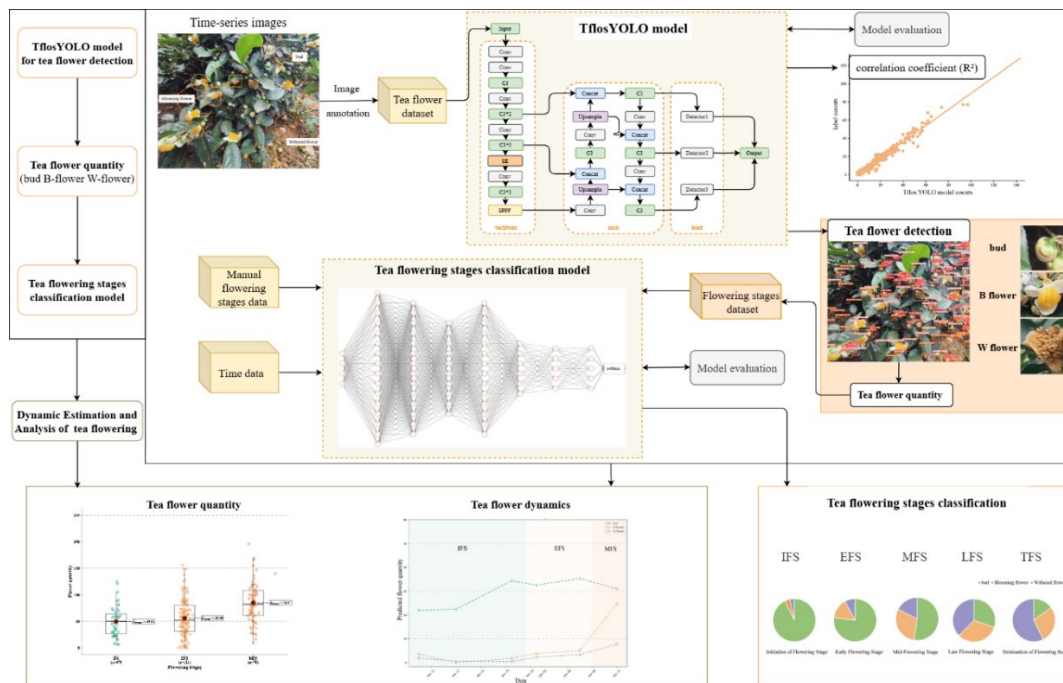


Fig. 1. Overall framework for dynamic estimation and analysis of tea flowering.

### 2.2 Study site and materials

The experimental data used in this study were obtained in November - December 2023 and October - December 2024 at the National Tea Germplasm Research Garden (Hangzhou). Hangzhou is located in the southeastern region of China (29°–30°N and 118°–120°E), within a subtropical monsoon climate zone. Our research involved 29 tea accessions originating from

different regions across the country, information on these accessions is provided in Table 2 and Table S1.

### **2.3 Data acquisition**

Tea plants in tea gardens are typically planted in rows with dense spacing between individual plants. Their flowers generally bloom predominantly on the sides of the plants. Considering this, we utilized mobile phone for image capture, as mobile phone photography offers flexibility, making it feasible for large-scale, cost-effective, and precise phenotypic monitoring. The mobile phone capture images in RGB color format as JPG files. The image resolution is 3280×2464 pixels, with a 72 dpi setting. The actual area corresponding to the regions captured in each image was calculated using Fiji[35] and is approximately 3690.33 cm<sup>2</sup> (69.26cm × 53.28cm per image), detailed method is shown in Figures S1. In order to enhance the generalization ability of the model, images in the complexity environments were collected in 2023-2024, including different lighting (e.g., backlight and frontlight), 29 tea accessions, various flowering densities, and both pruned and unpruned tea plants. In total, over 14,151 images were taken.

To evaluate the reliability of our approach as a substitute for traditional manual measurement and to explore the relationship between manual investigations and this framework, we conducted manual assessments of flower quantity and flowering stages after image collection. The method of manual assessments is illustrated in Fig. S2.

### **2.4 Images annotation and dataset analysis**

#### *2.4.1 Images annotation*

The original images captured by mobile phones had a resolution of 3280×2464 pixels. The input image size for the YOLO (You Only Look Once) model was determined based on the specific model configuration and task requirements. In this study, the input size for model training, validation, and testing was set to 640×640 pixels. To ensure compatibility with this input size and reduce computational cost, the original images were cropped into four sub-images, each with a size of 1640×1232 pixels. Image annotation was performed using LabelImg[36] in YOLO format. The labeled images were divided into three datasets for training, validation, and testing, following a 6:2:2 ratio. Three categories were defined for annotation: buds, blooming flowers (B flower), and withered flowers (W flower) (Fig. S3). In total, 28,668 instances were labeled across 2,361 images in the tea flower dataset (comprising the training, validation, and testing dataset). Additionally, various additional test datasets were constructed after annotation to assess the model performance.

#### 2.4.2 Dataset analysis for YOLO detection model

Three datasets were constructed for the training, validation, and testing of the tea flower detection model. The final annotated dataset included 2,361 images with a total of 28,668 instances: 16,392 (57%) were buds, 7,251 (25%) were blooming flowers (B flower), and 5,025 (18%) were withered flowers (W flower). Notably, buds accounted for the majority (57%) of the instances, while withered flowers represented only 18%, indicating a class imbalance in tea flower dataset (Table. 1, Fig. S4). To ensure reliability, generalization capability, and robustness of tea flower detection model, the tea flower dataset includes images from 26 tea accessions originating from six provinces of China (Table 2).

Table. 1. The amount of different classes in tea flower dataset.

<b>class</b>	<b>Training set</b> (1432 images)	<b>Validation set</b> (469 images)	<b>Test set</b> (460 images)	<b>All instances</b>
bud	9447	3300	3645	16392
Blooming flower	4303	1410	1538	7251
Withered flower	2905	996	1124	5025
All class	16655	5706	6307	28668

Table 2. Data samples of different accessions in tea flower dataset.

Origin province	Accession	Training set	Validation set	Test set	All
Hunan	Wannong 95 (WN95)	32	17	20	69
	Zhuyeqi (ZYQ)	50	20	5	75
	Gaoyaqi (GYQ)	99	29	5	133
	Baihaozao (BHZ)	30	18	33	81
	Jianbohuang (JBH)	11	6	5	22
Anhui	Anhui 1 (AH1)	44	17	28	89
	Anhui7 (AH7)	38	7	14	59
	Fuzao 2 (FZ2)	29	3	12	44
	Shuchazao (SCZ)	63	15	23	101
Jiangxi	Damianbai (DMB)	73	18	31	122
	Ningzhou 2 (NZ2)	151	53	18	222
	Shangmeizhou (SMZ)	156	55	36	247

Jiangsu	Xicha 5 (XC5)	65	11	15	91
Fujian	Echa 1 (EC1)	18	8	8	34
	Fuding Dahaocha (FDDH)	29	6	8	43
	Fu'an Dabaicha (FADB)	39	13	12	64
	Zhenghe Dabaicha (ZHDB)	73	20	29	122
	Fuyun 6 (FY6)	14	9	9	32
	Tie guanyin (TGY)	36	4	10	50
	Huang guanyin (HGY)	43	11	22	76
	Huang jingui (HJG)	55	13	23	91
	Huangqi (HQ)	33	8	12	53
	Mingke 1 (MK1)	43	14	10	67
	Maoxie (MX)	73	30	29	132
	Yuemingxiang (YMX)	50	21	19	90
Yunnan	Xicha 11 (XC11)	76	35	12	123
<b>all</b>		<b>1423</b>	<b>461</b>	<b>448</b>	<b>2332</b>

Moreover, 34 additional test datasets were constructed to evaluate the model on various tea accessions, flowering stages, lighting conditions (backlight and front light), and unpruned tea plant images. The frontlight and backlight test sets were collected from the same tea plot. Except unpruned test set, all test dataset constructed by pruned tea plants images. The image sizes for all training, validation, and test sets, as well as the 34 additional test datasets, have a size of  $1640 \times 1232$  pixels. The representative images and the amount of images for 34 additional test datasets have been provided in Fig. S5, Table S2.

## 2.5 TflosYOLO model for tea flower detection

### 2.5.1 YOLOv5 model

Although YOLOv7[37] has also shown excellent performance on agricultural datasets, considering the trade-off between model accuracy and computational cost, we adopt YOLOv5m as the baseline model for further improvement, aiming to achieve accurate and efficient tea flower detection across various environments and accessions while minimizing computational costs. This study utilizes YOLOv5 version 7.



The YOLOv5 network consists of three main components: (a) Backbone: CSPDarknet, (b) Neck: PANet, (c) Head: YOLO Layer. Initially, data is passed through the CSPDarknet for feature extraction. Next, it is processed through PANet to achieve feature fusion. Finally, the YOLO layer performs object detection and classification, outputting the final results in terms of detected objects and their corresponding classes.

In the detection process of YOLO-based algorithms, the input image is processed to generate feature map, which is divided into an  $S \times S$  grid. For each grid cell, anchor boxes are scored and boxes with low scores are discarded. Non-Maximum Suppression (NMS) is then applied to eliminate redundant boxes. Only the remaining boxes, along with their confidence scores, are retained and displayed. The confidence score is calculated as:

$$\text{confidence score} = \text{Pr}(\text{object}) * \text{IoU}(\text{pred}, \text{truth}) * \text{Pr}(\text{class}) \quad (1)$$

Where:

- $\text{Pr}(\text{object})$  represents the probability that an object exists,
- $\text{IoU}$  represents the Intersection over Union between the predicted and ground truth boxes,
- $\text{Pr}(\text{class})$  represents the probability that the predicted box belongs to each class.

$\text{IoU}$  is Area of Intersection. The  $\text{IoU}$  is calculated as:

$$\text{IOU} = \frac{\text{area}(B_p \cap B_{gt})}{\text{area}(B_p \cup B_{gt})} \quad (2)$$

$B_p$  is predicted bounding box,  $B_{gt}$  is ground truth box.

The YOLOv5 loss function consists of three components: classification loss, objectness loss, and box loss. To compute the total loss, these three components are combined as a weighted sum, which is expressed as follows:

$$\text{Loss} = w_{\text{box}} l_{\text{box}} + w_{\text{obj}} l_{\text{obj}} + w_{\text{cls}} l_{\text{cls}} \quad (3)$$

- $l_{\text{box}}$  is the box regression loss, which measures the difference between the predicted and ground truth box locations,
- $l_{\text{obj}}$  is the object confidence loss, which evaluates the accuracy of the model's object detection,
- $l_{\text{cls}}$  is the classification loss, which measures the model ability to classify the detected objects accurately.

## 2.5.2 TflosYOLO model

### 2.5.2.1 Challenges in tea flower detection

There are multiple challenges in tea flower detection as shown in Fig. 2. The field environment of tea garden is complex, with varying light conditions, backgrounds, and other factors contributing to significant background noise. In addition to this, tea flowers are small and tend to grow on the side of the tea plant densely, with buds and flowers often obscuring each other, prone to being obstructed or fragmented by branches and leaves, and they are also easily influenced by background flowers. These factors make tea flower detection more challenging compared to the detection of fruits like apples[10]. Furthermore, intermediate forms exist between buds, blooming flowers, and withered flowers, which are difficult to differentiate and can lead to a decrease in detection accuracy. Additionally, light interference, such as light spots, can cause buds to be misidentified. Detection accuracy is particularly affected by direct or strong light. The imbalance among different flower categories is also one of the challenges as the total number of tea buds and blooming flowers is significantly greater than the number of withered flowers. To address these challenges, this study proposes the TflosYOLO model, which aims to improve the accuracy of tea flower detection under various environmental conditions.

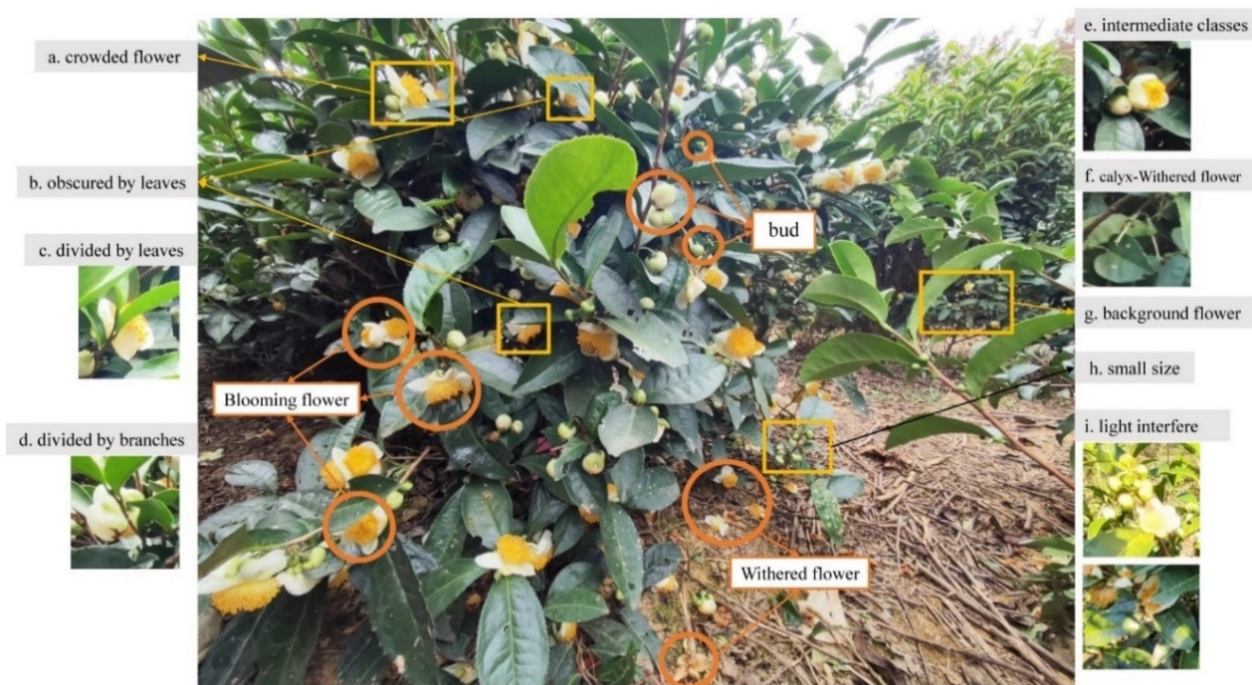


Fig. 2. Examples of the inflorescences on tea plant and difficult issues in tea flower detection. (a) crowded flower obscured by each other. (b) tea flower obscured by leaves. (c) tea flower divided by leaves. (d) tea flower divided by branches. (e) intermediate classes. (f) calyx belong to Withered flower, which can be easily detected as bud. (g) background flower that do not belong to the detected tree. (h) small size detection target. (i) light interfere.

### 2.5.2.2 Architecture of TflosYOLO model

In this study, the YOLOv5m model is used as the baseline. Modifications to the model's depth and width are made, and the SE (Squeeze-and-Excitation Networks) attention module is integrated into the backbone of YOLOv5. The SE module is added to the seventh layer of the YOLOv5 backbone, which enhances the model ability to handle complex backgrounds and lighting variations. The TflosYOLO model achieves high tea flower detection accuracy with relatively low computational cost, offering excellent generalization and robustness. The architecture of the TflosYOLO model (Fig. 3A) includes the backbone (CSPDarknet-53), the feature fusion neck, and the final detection layers.

The images are input into the TflosYOLO model, with the input size scaled to  $640 \times 640$  (input size for detection varies depending on image size). The images pass through the main feature extraction network of the TflosYOLO model, generating various feature maps. These feature maps undergo further subsampling and feature fusion in the neck section, integrating shallow and deep features. The C3 modules at layers 18, 21, and 24 output feature maps of sizes  $80 \times 80$ ,  $40 \times 40$ , and  $20 \times 20$ , respectively, for detecting small, medium, and large targets. The model divides the image into grids and generates anchor boxes of varying sizes and densities. Anchor boxes with high scores (including both object and category scores) are retained, and non-maximum suppression (NMS) is applied to eliminate redundant anchor boxes. The remaining anchor boxes are displayed on the image along with their predicted class confidences, providing the detection results for tea flower buds (bud), blooming flowers (B-flower), and withered flowers (W-flower), which are then used to output flower quantities.

### 2.5.2.3 Key Improvements in the TflosYOLO Model

This model introduces three primary improvements over the YOLOv5s model: Data Augmentation, YOLOv5 Model Scaling, integration of the SE Module.

The training images are augmented with mosaic, flipping, translation, and color enhancement techniques to address the problem of insufficient training data, particularly for withered flower samples, which could lead to model underfitting.

The YOLOv5 model includes several variants (YOLOv5s, YOLOv5m, YOLOv5l, YOLOv5x), all with identical model structures but differing `depth_multiple` and `width_multiple` parameters. The `depth_multiple` controls the number of modules, while `width_multiple` adjusts the number of convolution kernels to control the number of channels. In this study, we adjust both parameters, resulting in a model size between YOLOv5s and YOLOv5m, with performance superior to all versions (YOLOv5s, YOLOv5m, YOLOv5l, YOLOv5x).

Additionally, the SE(Squeeze-and-Excitation Networks) module- a channel attention mechanism[38,39], is added to the seventh layer of the YOLOv5 model. The structure of SE is shown in Fig. 3B. The SE module consists of two key steps: Squeeze and Excitation. It dynamically adjusts the weights of different channel by learning the relationships between channels, in order to make the network focus on more important features while suppressing unimportant channels.

#### 2.5.2.4 Training Details

The model was trained for 300 epochs with a batch size of 8 and a learning rate of 0.01, using the SGD optimizer. The input image is resized to 640×640 pixels. The experimental setup and Environmental settings: The operating system used was Ubuntu 18.04. The training was conducted on a single NVIDIA RTX 3080 GPU with 10GB of memory. The CPU utilized was an Intel Xeon Platinum 8255C. The software environment included PyTorch-cuda=11.8, CUDA 11.3, and Python 3.8.

#### 2.5.3 model evaluation

In order to assess the model for tea flower detection, eight key performance indicators (KPIs) are adopted in this study. Precision and Recall are commonly used evaluation metrics in deep learning Algorithm Evaluation, all of which are based on the confusion matrix[40]. The confusion matrix is presented in Table S3.

Precision is the proportion of True Positive (TP) in all detection- predicted positive samples (TP + FP). The formula is as fronts:

$$\text{Precision} = \frac{\text{TP}}{\text{TP}+\text{FP}} = \frac{\text{TP}}{\text{all detections}} \quad (4)$$

Recall is the proportion of True Positive (TP) in all actual positive samples (TP + FN). The formula is as fronts:

$$\text{Recall} = \frac{\text{TP}}{\text{TP}+\text{FN}} = \frac{\text{TP}}{\text{all actual positive}} \quad (5)$$

F1-score combines Precision and Recall to measure the performance of a model. The formula is as fronts:

$$\text{F1} = 2 \times \frac{\text{P} \times \text{R}}{\text{P} + \text{R}} \quad (6)$$

Where R is Recall and P is Precision, C denotes class.

In object detection algorithms, Intersection over Union (IoU) is a commonly used metric to evaluate the accuracy of predicted bounding boxes against ground truth boxes. IoU Threshold is a predefined value (commonly 0.5) used to determine whether a predicted bounding box is considered

a true positive. If the IoU between the predicted box and the ground truth box meets or exceeds this threshold, the prediction is counted as correct.

The formula is as follows:

$$\text{IOU} = \frac{\text{area}(B_p \cap B_{gt})}{\text{area}(B_p \cup B_{gt})} \quad (7)$$

Where  $B_p$  is predicted bounding box,  $B_{gt}$  is ground truth box.

Average Precision (AP) is a key metric used to assess the performance of detection models over one class, reflecting the trade-off between precision and recall. Specifically, mAP (mean Average Precision) averages the AP across different classes, providing a comprehensive evaluation of the model's ability to detect objects accurately. mAP0.5 refers to the mAP calculated at an IoU threshold of 0.5, commonly used to measure the model's performance under lower IoU; mAP0.5-0.95 represents the mean Average Precision calculated across a range of IoU (Intersection over Union) thresholds from 0.5 to 0.95, commonly used to measure the model's performance under higher IoU.

Formulas are provided below:

$$\text{AP} = \int_0^1 P(R) dR \quad (8)$$

$$\text{mAP} = \frac{\sum_{n=0}^c \text{AP}(C)}{C} \quad (9)$$

Where R is Recall and P is Precision, C denotes class.

Additionally, detection speed is used to evaluate detection time cost, while total parameters, FLOPs, and model size are crucial for evaluating model complexity and computational cost.

The coefficient of determination ( $R^2$ ) is a statistical measure that indicates the proportion of the variance in one variable that can be explained by the variance in another variable. In this study, we use  $R^2$  coefficient to assess the strength of the correlation between the manually observed, annotated, and predicted tea flower numbers, further validating the reliability of tea flower detection model.

Formula for  $R^2$  calculating are provided below:

$$R^2 = 1 - \frac{\sum_{i=1}^n (y_i - \hat{y}_i)^2}{\sum_{i=1}^n (y_i - \bar{y})^2} \quad (10)$$

where n is the number of samples,  $y_i$  is the manually observed or annotation flower quantity, and  $\hat{y}_i$  is the predicted tea flower quantity from deep learning model, and  $\bar{y}$  is the average of  $y_i$ .

## 2.6 tea flowering stages classification model

This study constructs a tea flowering stages classification model -TFSC model based on Artificial Neural Networks (ANN) and time-series images to enable precise dynamic monitoring of the

flowering period, addressing previous issues with inaccurate observation and inconsistent standards for tea flower phenotyping. Artificial Neural Networks (ANN), also known as Multilayer Perceptron (MLP), consist of fully connected layers. The input layer is the first layer, fronted by one or more hidden layers, and the final output layer. Each layer contains multiple artificial neural units (neurons).

### *2.6.1 Flowering stage dataset construction*

The tea plant flowering stage is categorized into five stages: IFS, EFS, MFS, LFS, and TFS. To construct the training and validation datasets, we utilized uncropped raw images of tea flowers collected in 2023. Recognizing that the flowering periods of tea plants are influenced by climatic factors and can vary significantly between years for the same variety, we incorporated tea flower images collected in 2024 to establish the test dataset. This test dataset, comprising 387 samples, aims to further validate the accuracy and generalizability of the flowering stage detection model.

Using the TflosYOLO model, we estimated the corresponding flower number (including the number of flower buds, B-flower, and W-flower) for each image. Additionally, we incorporated manually recorded flowering stage categories and time data. Each image's flower quantity, along with the manually observed flowering stage and time data, constituted a flowering stage sample, collectively forming the original flowering stage dataset.

Subsequently, we preprocessed the original flowering stage dataset by first filtering out low-quality data. This involved removing images of varieties with insufficient flower counts, as they could not provide reliable flowering stage assessments. For the remaining samples from the same time and accession, we calculated the average value from every three samples to create a new sample. This approach mitigates the influence of extreme cases and reflects the overall flowering characteristics of the accession. Each sample was then manually labeled with tags that included IFS, EFS, MFS, LFS, and TFS. The 2023 flowering period data was divided into training and validation sets in an 8:2 ratio, while the 2024 images served as the test set. The flowering stage dataset encompasses samples from 29 different tea accessions, representing various flowering stages.

### *2.6.2 TFSC model design and training*

The Flowering stage classification model is built based on ANN and the flowering period dataset. The tea flower detection model outputs are then processed by the flowering period model for automatic classification. The model is implemented using the PyTorch framework, with ReLU activation functions, softmax for classification, cross entropy loss and the Adam optimizer.

Key training parameters are as follows: The training involved a total of 3,667 samples, with 671 samples used for validation and 387 samples reserved for testing. The batch size was set to 16, and the learning rate was configured at 0.001. The model was trained for 80 epochs. The software environment utilized included PyTorch-cuda=11.8, CUDA 11.3, and Python 3.8.

The Flowering stage classification model is structured as a 7-layer neural network, shown in Fig. 3C. The input includes the number of buds, blooming flowers, and withered flowers, as well as time information. The labels are manually recorded flowering stage. After passing through six hidden layers and the softmax function for classification, the final output is the predicted probability of each flowering stage class (IFS, EFS, MFS, LFS, TFS).

The softmax function is calculated as:

$$\hat{y}_j = \frac{\exp(o_i)}{\sum_k \exp(o_k)} \quad (11)$$

Where  $\hat{y}_j$  represents the predicted probability,  $o_i$  is the unnormalized prediction for the  $i_{th}$  output, and  $k$  is vector of predicted outputs. The softmax function ensures that the predicted outputs sum to 1, with each value in the range [0, 1].

The ReLU (Rectified Linear Unit) activation function is commonly used in artificial neural networks to introduce non-linearity and avoid issues such as gradient explosion and vanishing gradients. The ReLU function is defined as:

$$f(x) = \max(0, x) \quad (12)$$

### 2.6.3 Model evaluation

The accuracy is validated on the test set using the accuracy score function. The accuracy is calculated as:

$$ACC = \frac{TP+TN}{TP+TN+FP+FN} \quad (13)$$

Where TP, TN, FP, and FN represent true positives, true negatives, false positives, and false negatives, respectively.

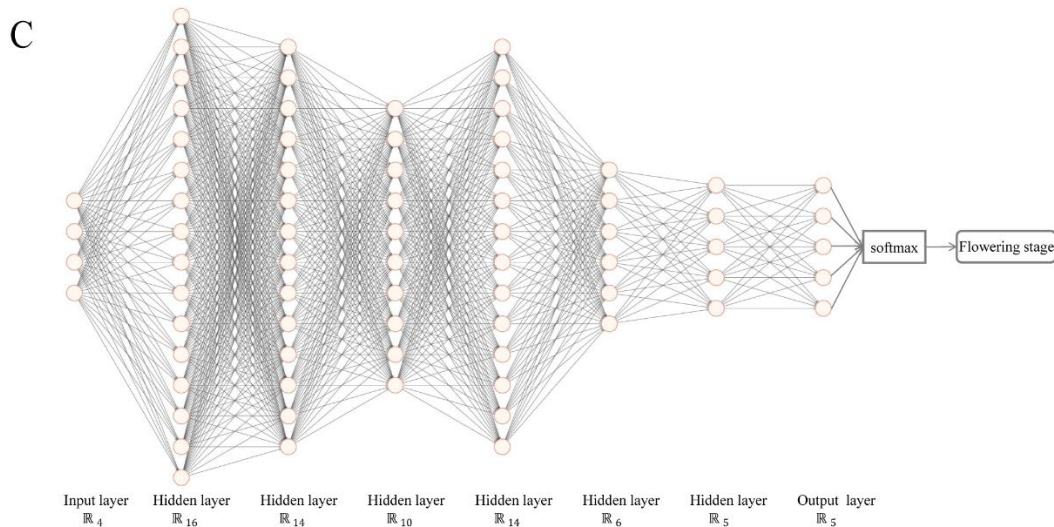
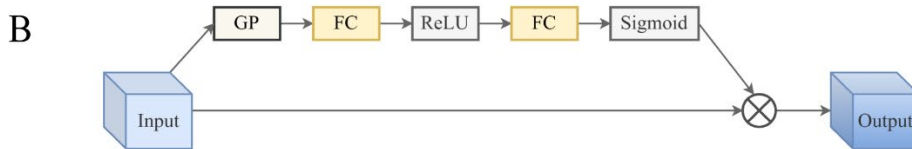
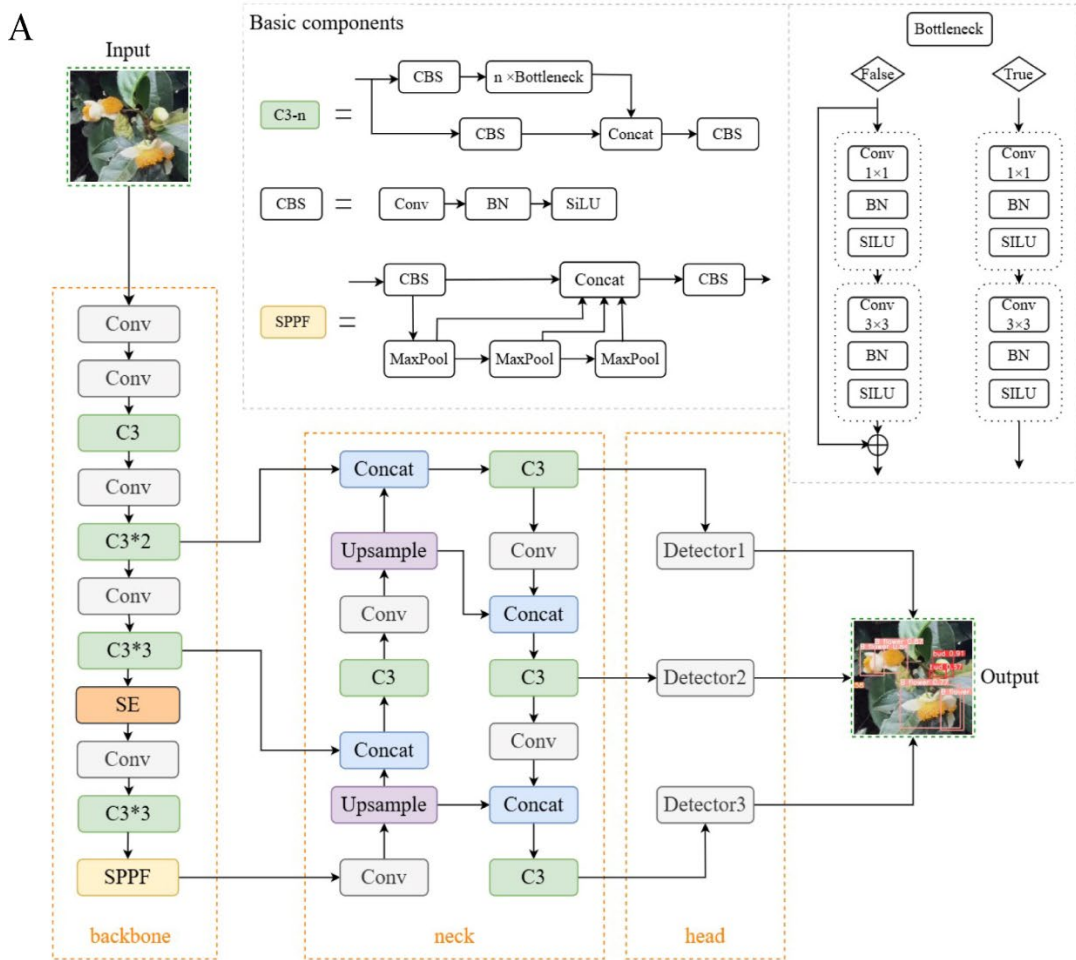


Fig. 3. The model structure in this study. (A) The architecture of the TflosYOLO model. (B) The structure of SE(Squeeze-and-Excitation Networks). GP = global pooling, FC = fully-connected layer. (C) The TFSC model (Tea flowering stage classification model) structure.



### 3. RESULTS

#### 3.1 TflosYOLO model performance and comparison

##### 3.1.1 TflosYOLO model performance for tea flower detection

The model performance was evaluated using test dataset, and the results are summarized in Table. 3. The TflosYOLO model can accurately detect and locate tea flowers. For the three categories, the mAP50 was 0.874, precision was 0.802, recall was 0.854, and the F1 score was 0.827. The mAP50 for flower buds, blooming flower, and withered flowers all exceeded 0.82, with bud achieving the highest detection accuracy (mAP50 = 0.913). The precision, recall, and F1 scores for bud and blooming flower were all above 0.80. While the performance for withered flower was slightly lower, it still exceeded 0.76. These results demonstrate that the model exhibits high accuracy and generalization capability. The model detection performance on one image is provided in Fig. S6, showing that TflosYOLO can accurately detect and locate tea flowers, even when they are obstructed by branches and leaves or when partial occlusions occur between flowers and bud. Additionally, mAP50 of TflosYOLO model on validation dataset set was 0.808(Table S4).

Table. 3. Performance of the TflosYOLO model based on test dataset.

Class	Precision	Recall	F <sub>1</sub> -score	mAP50	mAP50-95	Params	Model_size	GFlops
						/M	/M	
all class	0.802	0.854	0.827	0.874	0.696	15.8	30.4	34.9
bud	0.835	0.885	0.859	0.913	0.737			
B flower	0.801	0.867	0.833	0.881	0.685			
W flower	0.769	0.810	0.789	0.827	0.666			

##### 3.1.2 Evaluating the robustness of TflosYOLO model

To assess the robustness and generalization ability of the TflosYOLO model, 34 additional test datasets were used, covering 26 tea accessions and 5 flowering stage datasets: IFS, EFS, MFS, LFS, TFS, along with test set from unpruned tea plants and both backlight and frontlight conditions. The detailed composition of 34 test dataset is provided in Table S2. The test results as shown in Fig. 4 presents the precision, recall, and mAP50 values for the TflosYOLO model across 34 additional test datasets, whole indicates results from test dataset.

The model performed slightly less effectively for accessions with very few flowers, such as EC1 and FY6, with mAP50 values reaching 0.74 or higher. For the majority of accessions, the mAP50 exceeded 0.8, and for several accessions, it was above 0.9. To prevent lengthiness, detailed results regarding the performance of TflosYOLO model on 34 test set have been provided in Table S5, 6, 7. The model performed best during the PFS (including EFS, MFS, LFS), with LFS showing the most accurate predictions, while IFS and TFS had the lowest accuracy (Fig. 4A, Table S5, S7). In

particular, accuracy and recall for blooming flower and withered flower in the IFS were low, as accuracy and recall for bud in the LFS and TFS were also relatively low. All tea plants in the test dataset (whole) are pruned. The model performed slightly better on pruned tea plants compared to unpruned ones, but accuracy, recall, and F1 scores for both pruned and unpruned datasets exceeded 0.8. The model's performance under frontlight conditions was noticeably lower than under backlight, but the mAP50 remained above 0.8 under both conditions. In summary, accuracy of TflosYOLO model across most accessions, flowering stages, pruned and unpruned tea plants, and varying light conditions remained above 0.8, indicating high robustness and generalization capability.

### *3.1.3 Correlation Analysis*

To further evaluate reliability of TflosYOLO model, correlation analysis was conducted using the  $R^2$  coefficient. The correlation between the predicted flower count by TflosYOLO and the labeled flower count was computed based on the tea flower test dataset. The linear regression between the predicted flower count by TflosYOLO and the actual flower count (from labeled data) is shown in Fig. 4B. The correlation coefficient ( $R^2$ ) for the predicted and actual flower count was 0.974, indicating a strong correlation between the predicted flower count and the actual count.

Additionally, the correlation between the predicted flower count and actual flower quantity levels from traditional manual surveys was analyzed. The flower count here refers to the sum of bud and blooming flowers in each image. As shown in Fig. 4C, the predicted flower count and flower quantity level from traditional manual investigation are basically consistent.

### *3.1.4 Ablation experiments of TflosYOLO model*

This study used YOLOv5m as the baseline model and incorporated various improvements into TflosYOLO to improve model performance in different environmental conditions. The ablation experiment was conducted based on the validation dataset (Fig. 4D). YOLOv5f modifies the depth and width of the YOLOv5 model, with depth and width multiplies of 0.33 and 0.75, respectively, placing it between YOLOv5s and YOLOv5m. Compared to the YOLOv5m model, YOLOv5f showed improvements in precision, recall, F1-score, mAP50, and mAP50-95, while the number of parameters, model size, and GFLOPs were significantly reduced, demonstrating increased accuracy with lower computational costs. Image enhancement (IE), which involved additional image augmentation, led to significant improvements in precision, recall, F1-score, mAP50, and mAP50-95 compared to YOLOv5f. The addition of the Squeeze-and-Excitation (SE) module further

enhanced the recall, F1-score, mAP50, and mAP50-95, with no change in the number of parameters, model size, or GFLOPs.

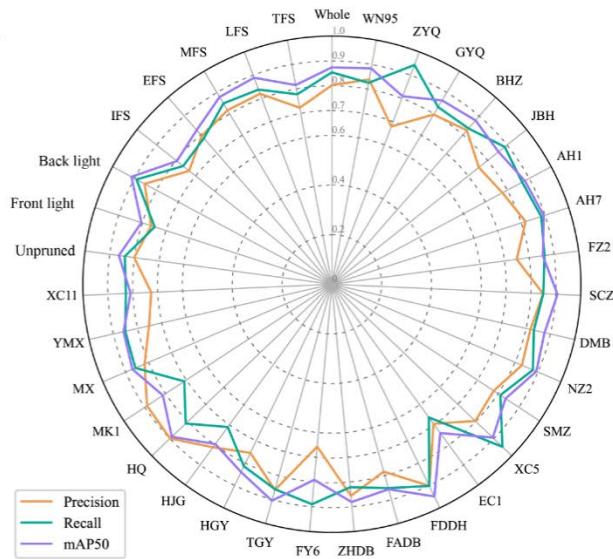
Table 4. The evaluation result of the ablation experiment.

Model	Precision	Recall	F <sub>1</sub> -score	mAP50	mAP50 -95	Params /M	Model_size /M	GFloPs
YOLOv5m	0.759	0.685	0.720	0.760	0.499	20.9	40.2	47.9
YOLOv5f	0.774	0.693	0.731	0.763	0.506	15.8	30.4	34.9
YOLOv5f+IE	0.795	0.712	0.751	0.793	0.490	15.8	30.4	34.9
YOLOv5f+IE +SE	<b>0.792</b>	<b>0.727</b>	<b>0.760</b>	<b>0.808</b>	<b>0.523</b>	15.8	<b>30.4</b>	<b>34.9</b>

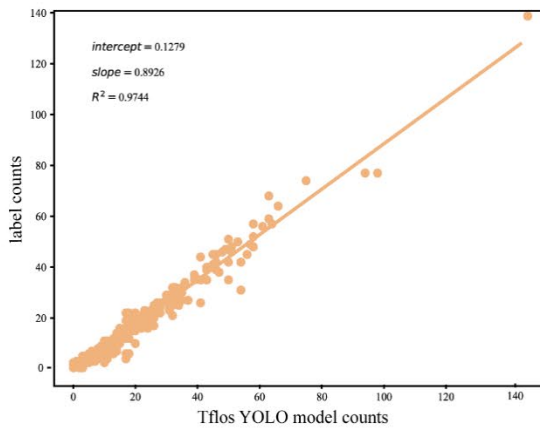
Two test images were selected for the ablation experiment comparison: one under backlight with medium light intensity and the other under frontlight on a sunny day. The areas of interest are highlighted in white circles (Fig. 4D). Under normal lighting conditions, the differences between models were minimal. However, with image enhancement, the TflosYOLO model correctly detect the flower calyx as a withered flower, whereas YOLOv5f misclassified it as a bud. Image enhancement and the SE attention module mitigated the issues caused by class imbalance, leading to more accurate detection of withered flowers. Under strong light and frontlight conditions, tea flower detection was interfered, with several objects missed by models in (a), (b) and (c) due to intense lighting. TflosYOLO showed superior performance under these conditions, detecting more buds and blooming flowers correctly.

In general, after the model improvements, the detection of withered flowers showed the greatest progress, fronted by blooming flowers, while improvements in bud detection were modest. The recall for withered flowers increased significantly, likely due to improved recall of flower calyxes, compensating for difficulties caused by data underfitting and class imbalance. TflosYOLO demonstrated noticeable improvements in detecting buds under strong light and also improved the detection of withered flowers. These model enhancements were beneficial in addressing challenges under strong light and frontlight conditions and were effective in mitigating class imbalance issues. Besides, the Squeeze-and-Excitation Networks contributed to model performance, generalization ability, and resistance to background noise.

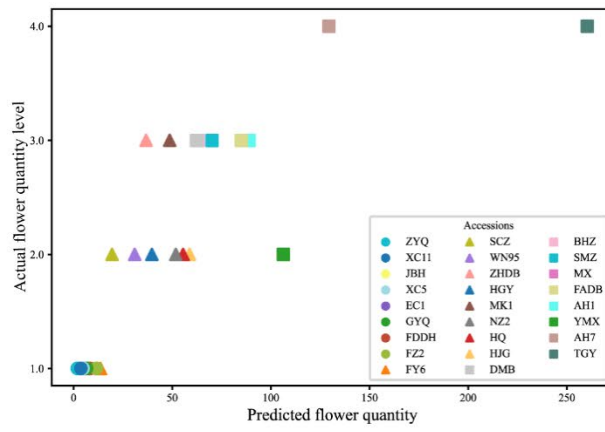
A



B



C



D

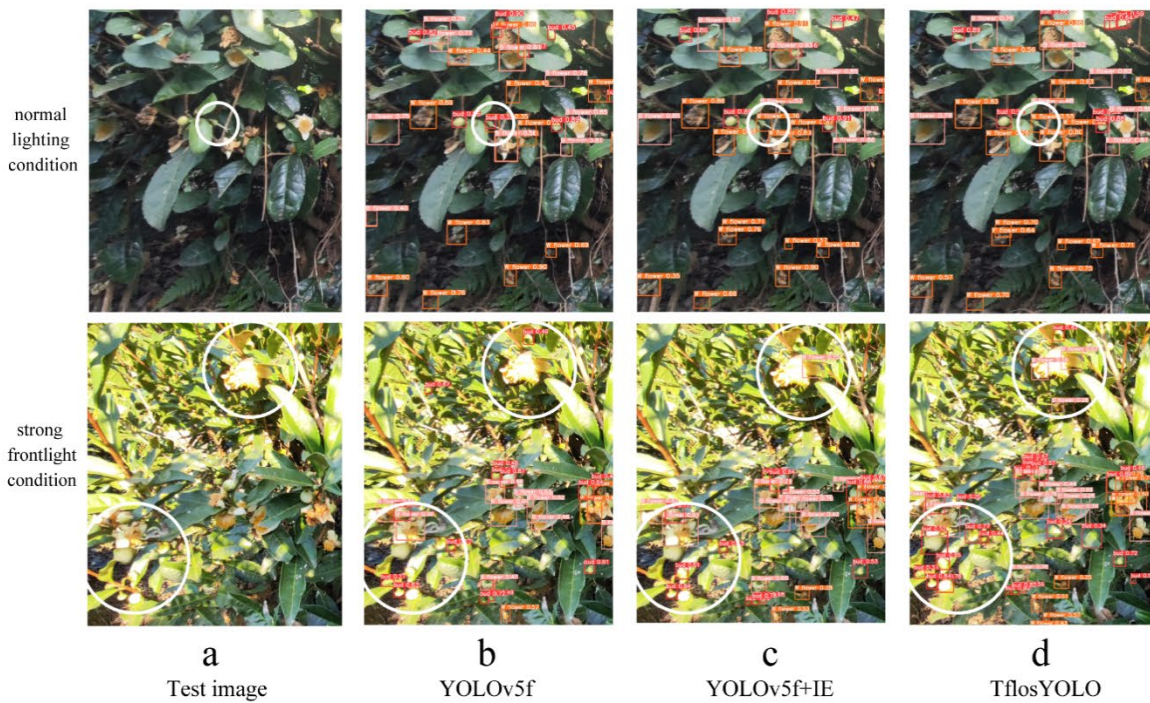


Fig. 4. The evaluation of TflosYOLO model performance. (A) The performance of TflosYOLO model on 34 additional test set. (B) The linear regression between the predicted flower count by TflosYOLO and the actual flower count (from labeled data). (C) The flower quantity comparison between the predicted flower quantity and actual flower quantity levels from traditional manual surveys across 26 accessions. (D) Comparison of the detection effect of model improvement: (a) Test image. (b) YOLOv5f, depth\_multiple=0.33, width\_multiple=0.75. (c) YOLOv5f+IE, IE denotes Image Enhancement. (d) TflosYOLO, which include YOLOv5f+IE+SE. SE is Squeeze-and-Excitation Networks. The white circle highlights the key areas that show differences in comparison.

### 3.1.5 Comparative performance of YOLO algorithms for tea flower detection

To compare the performance of the TflosYOLO model with other YOLO algorithms, we evaluated YOLOv5 (n/s/m/l/x), YOLOv7 (yolov7-tiny/yolov7/yolov7x), and YOLOv8 (n/s/m/l/x) models based on a validation dataset. The models were trained using the same parameters, and the results are summarized in Table 5, Fig. 5A, B. Compared to YOLOv5, YOLOv7, and YOLOv8, TflosYOLO performed better in detecting tea flowers, achieving higher precision, recall, and mAP50-95 while requiring fewer computational resources and having a model size between YOLOv5s and YOLOv5m. The table presents the average detection performance for the three classes-buds, blooming flower, and withered flowers.

Table 5. Comparison of YOLOv5(n/s/m/l/x) & YOLOv7(tiny/yolov7/x) & YOLOv8(n/s/m/l/x) model performance.

Model	Precision	Recall	F <sub>1</sub> -score	mAP50	mAP50-95	Params /M	Model_size /M	GFlops
YOLOv5n	0.764	0.663	0.710	0.738	0.441	1.8	3.68	4.1
YOLOv5s	0.778	0.683	0.727	0.764	0.459	7.0	13.7	15.8
YOLOv5m	0.759	0.685	0.720	0.760	0.499	20.9	40.2	47.9
YOLOv5l	0.819	0.669	0.736	0.748	0.481	46.1	88.5	107.7
YOLOv5x	0.770	0.725	0.747	0.779	0.526	86.2	165	203.8
YOLOv8n	0.740	0.653	0.694	0.734	0.452	3.0	6.2	8.1
YOLOv8s	0.752	0.679	0.714	0.752	0.468	11.1	22.5	28.4
YOLOv8m	0.734	0.682	0.707	0.750	0.461	25.8	52.0	78.7
YOLOv8l	0.737	0.665	0.699	0.743	0.454	43.6	250	164.8
YOLOv8x	0.745	0.673	0.707	0.735	0.458	68.1	136.7	257.4
YOLOv7tiny	0.762	0.687	0.723	0.748	0.455	6.0	12.3	13.2
YOLOv7	0.761	0.720	0.740	0.778	0.490	37.2	74.8	105.1
YOLOv7x	0.726	0.701	0.713	0.744	0.452	70.8	142.1	188.9
<b>TflosYOLO</b>	<b>0.792</b>	<b>0.727</b>	<b>0.760</b>	<b>0.808</b>	<b>0.523</b>	15.8	<b>30.4</b>	<b>34.9</b>

In conditions of bright light and front-light, TflosYOLO had a lower misidentification rate, accurately identifying flower buds and blooming flowers, while other models missed many flower buds or flowers under intense lighting (Fig. 5C). In environments with moderate lighting, performances among models were similar (Fig. S7), but TflosYOLO correctly identified the flower calyx as a withered flower, whereas other models either failed to detect the calyx or misclassified it as a flower bud. In conclusion, the TflosYOLO model demonstrated superior performance in detecting tea flowers under both strong light and front-light conditions as it has higher accuracy, particularly for bud and withered flowers, while other models struggle with these conditions.

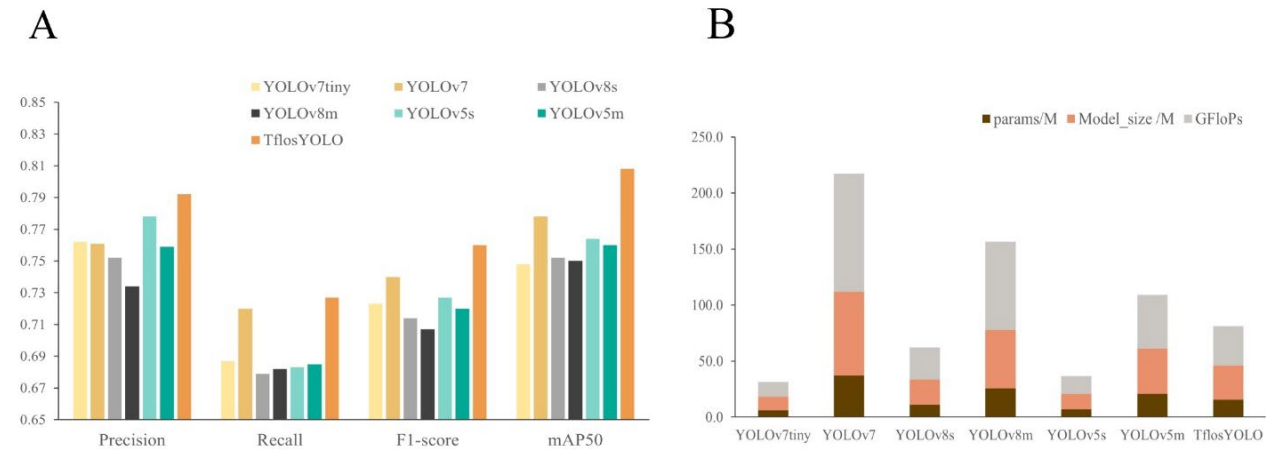


Fig. 5. Comparison of the TflorYOLO model with YOLOv5(n/s/m/l/x) & YOLOv7(tiny/yolov7/x) & YOLOv8(n/s/m/l/x) model. (A) Comparison of model accuracy. (B) Comparison of model size and efficiency. (C) Comparison of model performance under front-light condition on sunny day.

### 3.2 Evaluation of tea flowering stages classification model (TFSC)

The TFSC based on Artificial Neural Networks (ANN) achieved an accuracy of 0.738 and 0.899 on the validation dataset and test dataset respectively. The confusion matrix (Fig. 6) indicates that classification of the flowering stages is prone to misclassification between adjacent stages. Specifically, there is frequent confusion between the EFS, MFS, and LFS, as the agricultural dataset contains a large number of intermediate periods and intermediate-type samples. Such misclassification is common in manual classification as well, especially between adjacent stages.

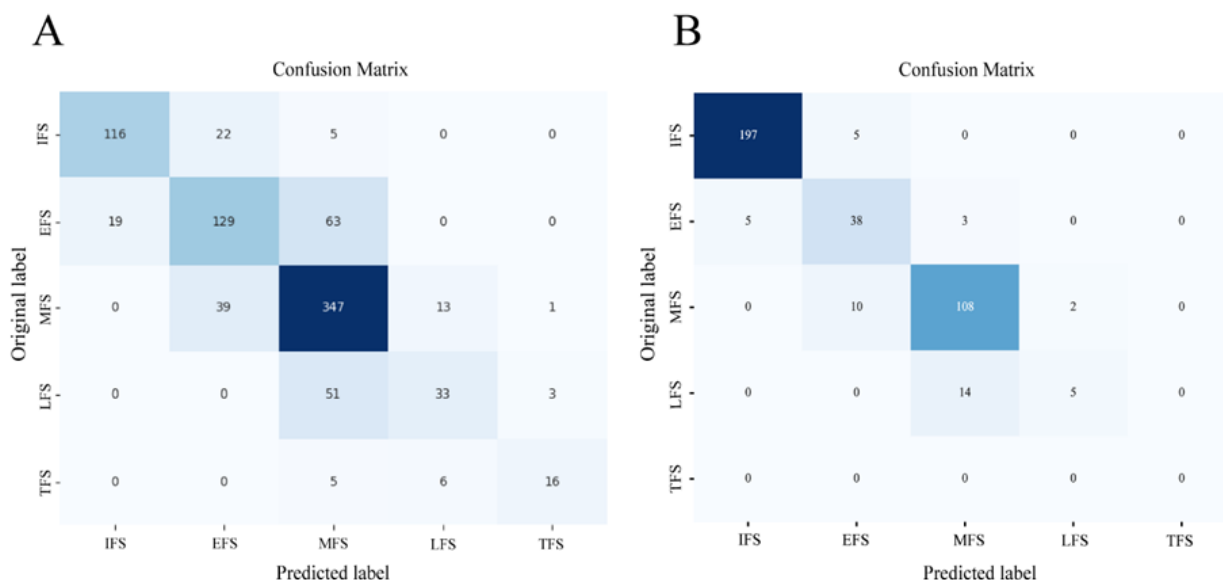


Fig. 6. The confusion matrix of predicted flowering stages and manual recorded flowering stages. Initial Flowering Stage (IFS), Early Peak Flowering Stage (EFS), Mid Peak Flowering Stage (MFS), Late Peak Flowering Stage (LFS), and Terminal Flowering Stage (TFS). (A) The confusion matrix based on validation dataset. (B) The confusion matrix based on test dataset.

### 3.3 Analysis of tea flower quantity and flowering stage

This section presents the estimation and analysis of tea flower quantity and flowering stages across various tea accessions, utilizing the established model.

#### 3.3.1 time-series dataset analysis for tea flowering observations

The composition of time-series dataset constructed for observing tea flowering dynamics including 29 tea accessions and 5 flowering stages in 2023-2024 was summarized (Table S8). The 29 tea accessions originated from provinces including Hunan, Anhui, Jiangxi, Jiangsu, Fujian, and Yunnan. The tea flowering observation dataset contains a total of 5,029 and 4345 images in 2023

and 2024, which were manually categorized into 5 flowering stages, images from the PFS account for the largest proportion, while the TFS contributes the smallest proportion. The TflosYOLO model was used to perform dynamic observations of flowering quantity and stage based on this dataset. The time-series dataset was not cropped, retaining more of the original image information, with images sized at 3280×2464 pixels. The actual area of each image is approximately 3690.33 cm<sup>2</sup> (69.26 cm × 53.28 cm). Each image contained flowers from two to three trees on one side. It is important to note that different tea accessions have significant differences in flowering time, and images taken at the same time may correspond to different flowering stages for different accessions.

In the tea flowering observation dataset, the proportion of buds, blooming flowers, and withered flowers at different flowering stages in 2023 is analyzed (Fig. 7A, Table S9). The proportion of buds gradually decreases over time, from 93% in the Initiation of Flowering Stage (IFS) to only 15% in the Termination of Flowering Stage (TFS). The proportion of withered flowers increases over time, from 3% in the Initiation of Flowering Stage to 57% in the Late Flowering Stage. Blooming flowers show a rising trend initially, then a decline, with their proportion staying above 30% in both the Mid-Flowering and Late Flowering Stages (Fig. 7A). We further analyzed the distribution of all blooming flowers across different flowering stages in 2023, where 72,085 blooming flowers were recorded in the PFS, representing 93% of the total blooming flowers (Fig. 7B).

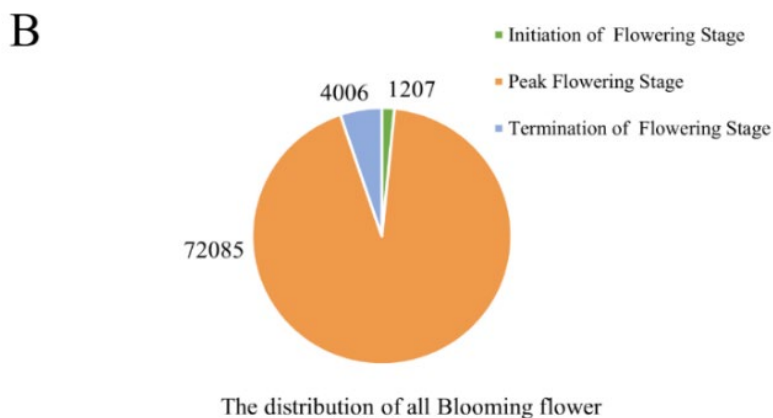
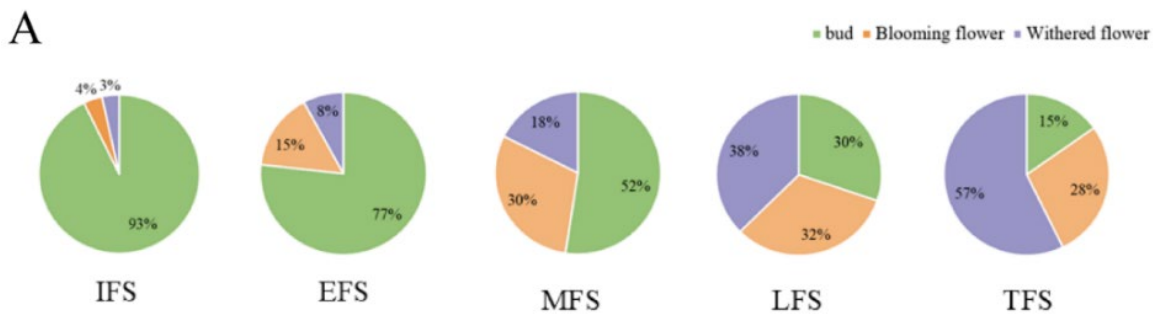




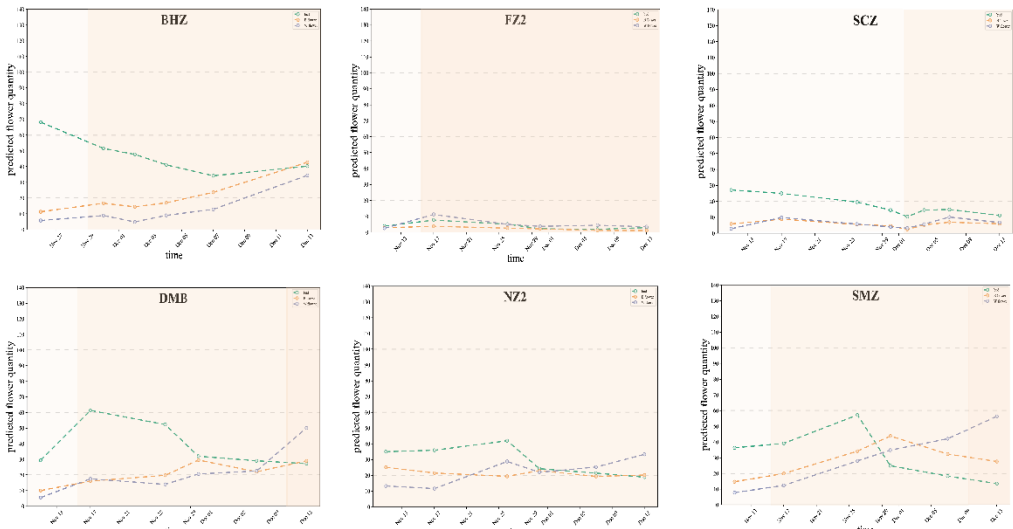
Fig. 7. The proportion of buds, blooming flowers, and withered flowers in 2023. (A) The proportion of bud, Blooming flower and Withered flower in the 2023 dataset for tea flowering observations across 5 Flowering Stage. (B) The distribution of all blooming flower in 2023 flowering stage.

### *3.3.2 Monitoring of tea flowering dynamics with flowering stage information*

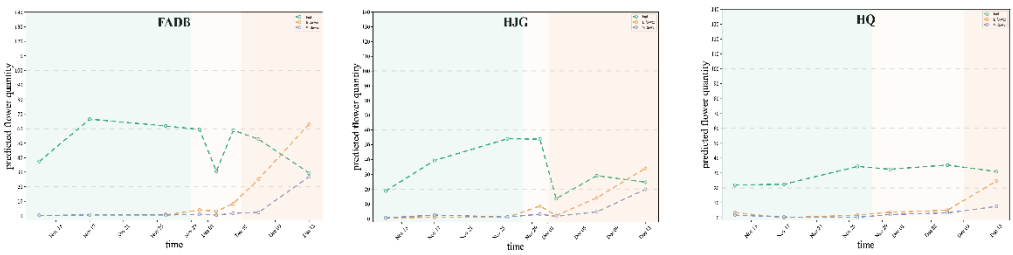
Using time-series images of 29 tea accessions in 2023, 2024 and the TflosYOLO model, we monitored the flowering dynamics of different tea accessions and used TFSC model to track the changes in flowering stages. The tea flowering dynamics of 9 tea accessions in November - December 2023 and October - December 2024, are shown in

Fig. 8, grouped according to different tea region and year. The tea flowering dynamics of other tea accessions in 2023 and 2024 are provided in Fig. S8, 9.

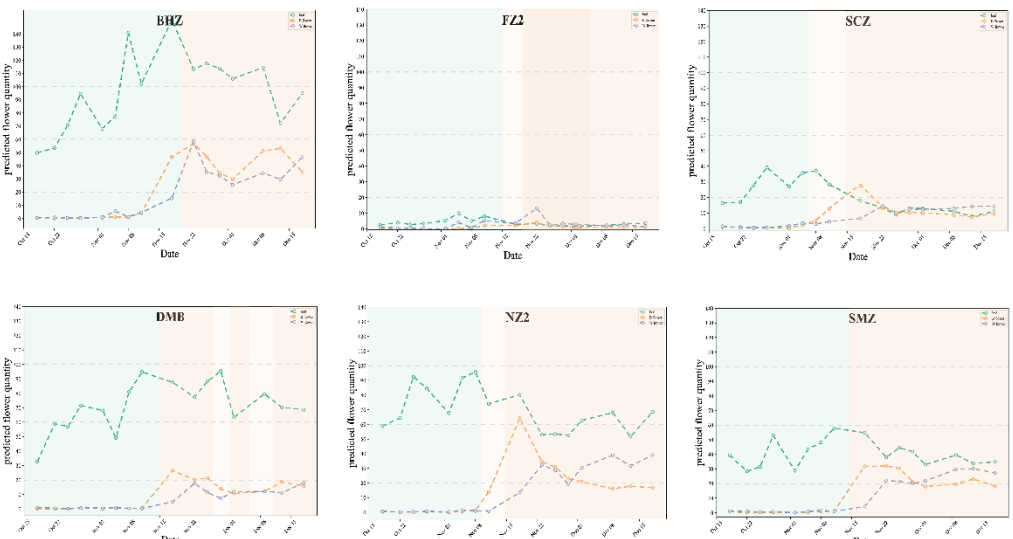
**A** 2023 IFS EFS MFS LFS TFS



**B**



**C** 2024 IFS EFS MFS LFS TFS



**D**

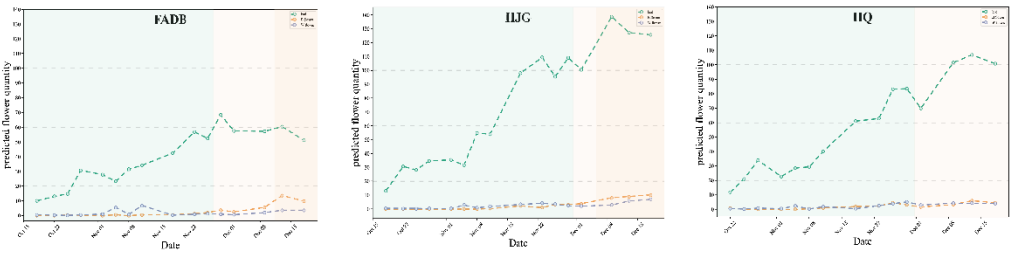


Fig. 8. Tea flowering dynamics and stage information for 9 accessions in November - December 2023 and October - December 2024. (A) The tea flowering dynamics of tea accessions from Southern Yangtze tea region in 2023; (B) The tea flowering dynamics of tea accessions from southern China tea region in 2023; (C) The tea flowering dynamics of tea accessions from Southern Yangtze tea region in 2024; (D) The tea flowering dynamics of tea accessions from southern China tea region in 2024.

The flowering dynamics of different tea accessions exhibited distinct differences. Overall, the quantity of buds increased during the IFS and then gradually decreased. The number of blooming flowers increased during the IFS and PFS, possibly exhibiting multiple peaks, and gradually decreased as the TFS approached. Withered flowers increased throughout the flowering period. Furthermore, accessions with closer genetic relationships displayed similar flowering timings and dynamics. For example, tea accessions from the Southern Yangtze tea region typically flower earlier, entering EFS in early November. In contrast, accessions from southern China tea region generally flower later, with several accessions such as HJG, HQ, and FADB still in IFS by late November. In 2024, the flowering period of tea plants was generally later than in 2023. Most accessions from the Southern Yangtze tea region entered the EFS after November 15, while accessions from the southern China tea region entered the EFS even later. Additionally, accessions from the Southern Yangtze tea region exhibited significantly longer PFS compared to others, which is consistent with previous studies indicating that accessions from the Southern Yangtze tea region tend to have longer flowering periods.

The relative early or late flowering of tea accessions is summarized in Table S10. With the exception of BHZ, the Flowering Stages predicted by the model aligned with those recorded manually. Accessions with very low flower quantities, such as XC11, were not included in flowering stage predictions.

### *3.3.3 Distribution of flower quantity across different tea accessions, year and conditions*

The tea flower detection model, TflosYOLO, was used to process time-series images of various tea accessions, providing flower quantity data for each accession at different flowering stages. The analysis and comparison of flower quantities across accessions were performed using data from the 2023-2024 Peak Flowering Stage (PFS) (Fig. 9A). The flower quantity of same accession is relatively consistent between the two years PFS. The accessions with the lowest flower quantities in this study were ZYQ, XC5, XC11, JBH, EC1, GYQ, FDDH, FZ2, LJ43 and FY6. Accessions with intermediate flower quantities in this study, include SCZ, WN95, ZHDB, HGY, MK1, NZ2, HQ, and HJG. Accessions with higher flower quantities, include DMB, BHZ, SMZ, MX, FADB, AH1, YMX, AH7, and TGY. Among these, TGY exhibited exceptionally high flower quantities,

with an average over 170 in 2 years, likely due to its sparse planting, resulting in excessive light exposure and consequently higher flower quantity.

To further validate the robustness and reliability of the model, flower quantity under backlighting (BL) and frontlighting (FL) conditions was compared (Fig. 9B, C). The comparison was performed for both backlighting and frontlighting Jin Xuan tea plants. The flower quantities under backlighting and frontlighting were similar, with no significant differences ( $p$ -value  $> 0.05$ ). The TflosYOLO model demonstrated stable performance under both lighting conditions, unaffected by lighting variations, indicating the model's strong robustness.

Additionally, a significant difference in flower quantity was observed between pruned and naturally growing tea plants. In this study, the flower quantity of both pruned and unpruned LJ43 tea plants was compared. The unpruned LJ43 plants exhibited significantly higher flower quantities than the pruned ones, with a  $p$ -value  $< 0.01$  (Fig. 9D). This aligns with previous studies, which also reported lower flower quantities in pruned tea plants.

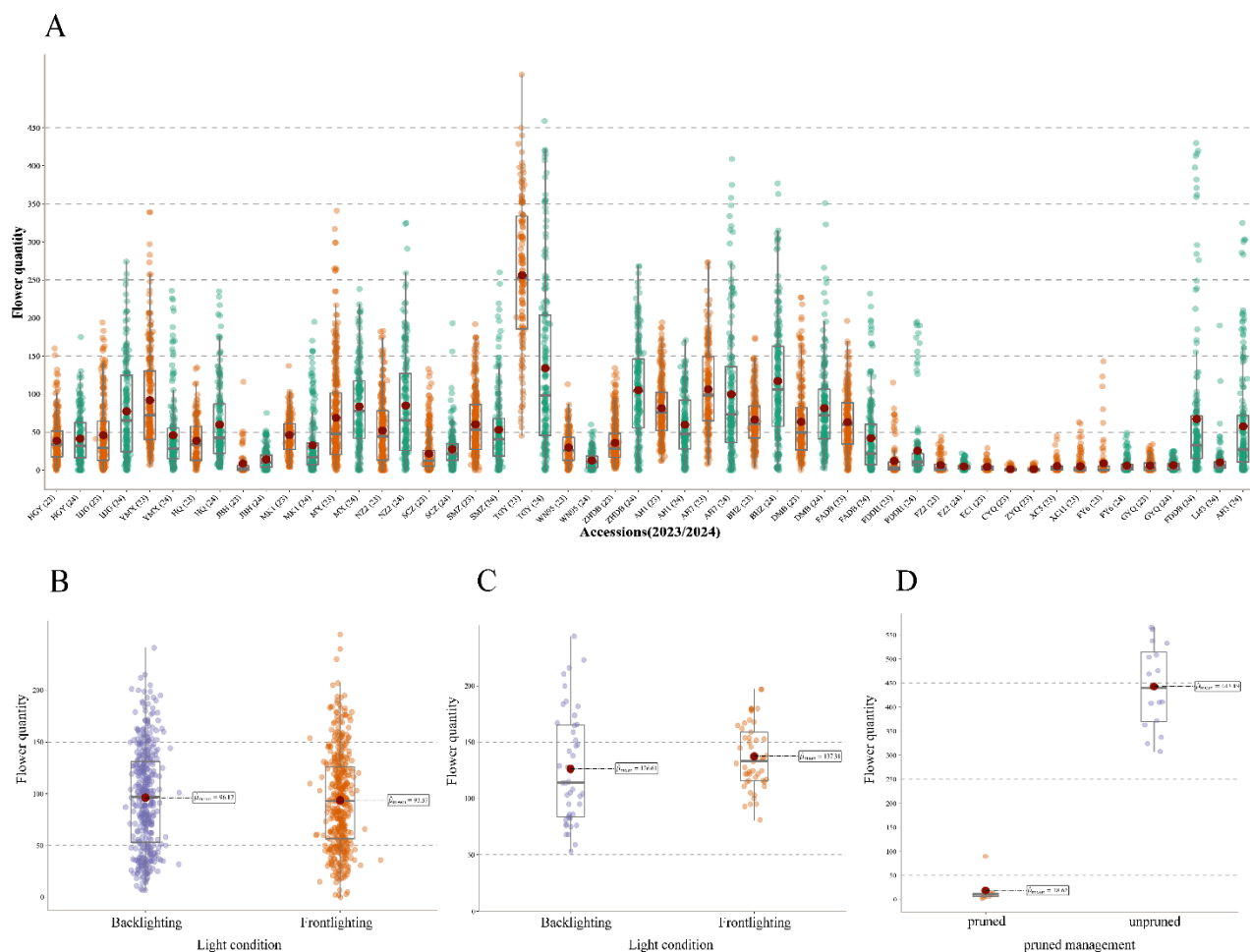


Fig. 9. Distribution of flower quantity across different tea accessions, year and conditions. (A) Distribution of flower quantity across 29 accessions (2023, 2024). Each point represents the flower quantity in a single image during the PFS, which contains the profile of 2-3 tea plants corresponding to the actual area of 3690.33 cm<sup>2</sup> (69.26

cm × 53.28 cm). Flower quantity is calculated as the sum of detected buds and blooming flowers. The red dot represents the mean flower quantity. (B) The comparison of flower quantity under frontlighting and backlighting conditions for tea plants from the same plot; (C) The comparison for Jin Xuan tea plants under frontlighting and backlighting conditions. (D) Distribution of flower quantity for LJ43: pruned vs. unpruned management.

### *3.3.4 Distribution of flower quantity across different tea flowering stages*

Additionally, flower quantity data for each flowering stage (IFS, EFS, MFS, LFS, TFS) were analyzed separately for accessions from Fujian provinces as shown in Fig. 10, data of accessions from other provinces is provided in Fig. S10. Significant variability in flower quantity was observed across different tea accessions, with accessions of closer genetic relationships showing more similar flower quantities regularly. For instance, accessions from Fujian, such as TGY, HJG, HGY, HQ, MK1, and YMX, exhibit similar flower quantities due to their close genetic ties. YMX, a descendant of TGY, and HQ, a hybrid of HJG, exhibit similar flower quantities due to their close genetic ties both exceeded 100 flowers in the MFS. The flowering quantity of the same accessions in 2023 and 2024 was relatively stable. For instance, TGY, MX, and YMX exhibited high flowering quantities in both years, while HGY had lower flowering quantities. However, due to climatic differences between 2023 and 2024, the flowering dynamics of the same accession varied, as exemplified by YMX, which had a later flowering stage in 2024 compared to 2023, along with a significantly lower flowering quantity. Additionally, variations in flowering quantities between different years can also be attributed to differences in management practices. For example, due to increased sunlight in 2024, ZHDB exhibited a significantly higher flowering quantity compared to 2023. Furthermore, the additional collection of images in October 2024, was also one of the factors contributing to the changes during the IFS and EFS.

Moreover, flower quantity dynamics during different flowering stages vary significantly. While most tea accessions do not show significant differences in flower quantity between the PFS (EFS, MFS, LFS), significant differences in flower quantity were observed between IFS, PFS, and TFS.

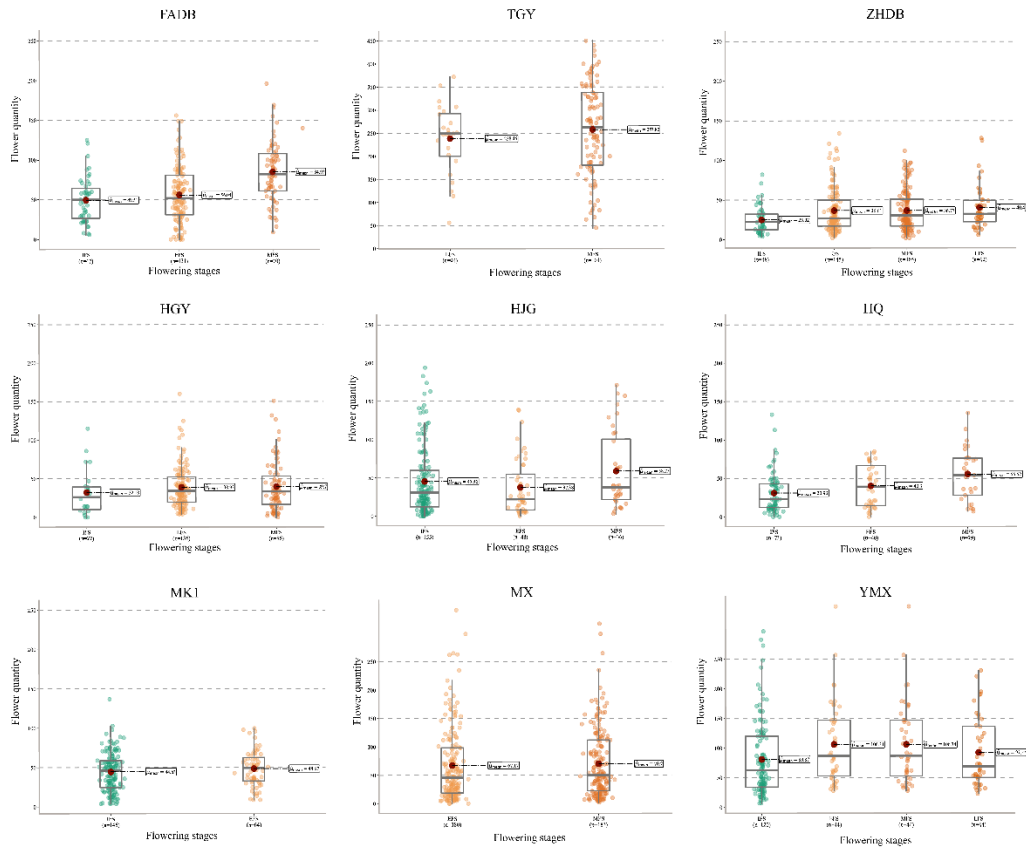
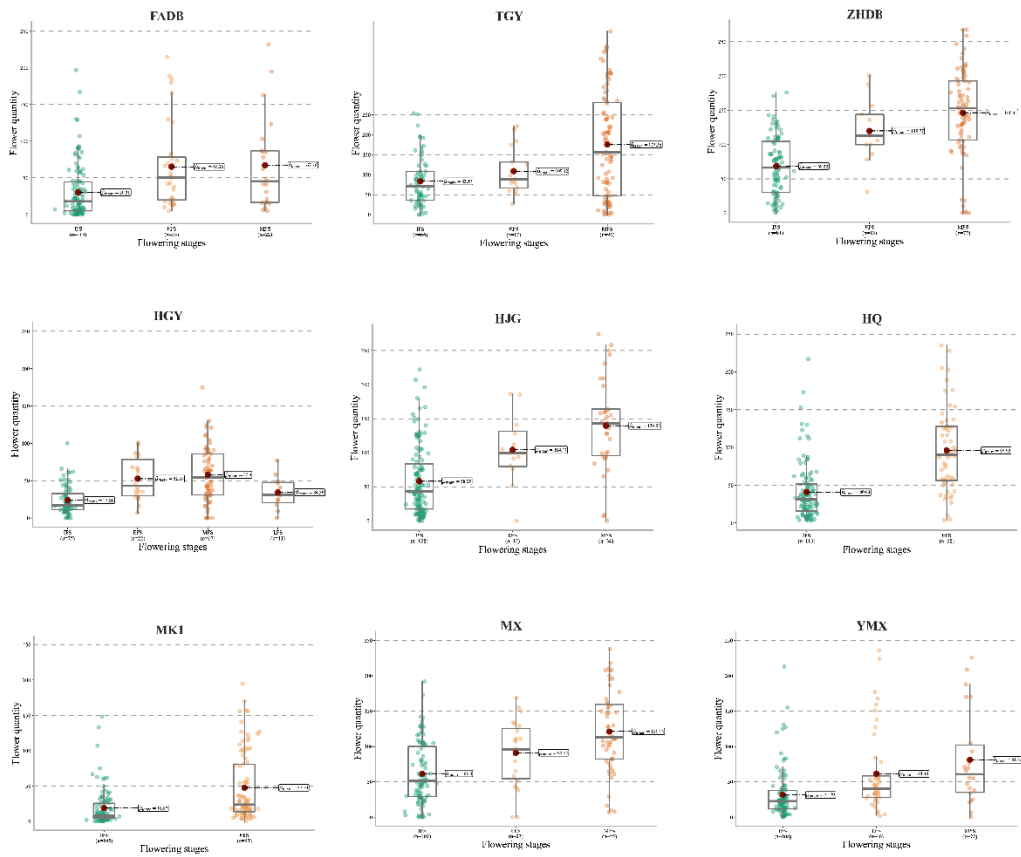
**A****2023****B****2024**

Fig. 10. Flower quantity data for each flowering stage (IFS, EFS, MFS, LFS, TFS) across 9 accessions from Fujian province. (A) November and December 2023. (B) October, November and December 2024.

## 4. DISCUSSION

### Importance of Datasets

Agricultural datasets typically present challenges such as significant background noise and small object sizes, making the model performance very different from the evaluations done using datasets like COCO. For example, in this study, YOLOv5s outperformed the more computationally intensive YOLOv5l x and even YOLOv8. In the training and construction of deep learning models, such as YOLO, the representativeness and diversity of the dataset are more crucial than improvements in the model architecture. The performance of model can vary significantly across different accessions. Therefore, achieving good results on a single dataset does not guarantee consistent performance across all scenarios, and it is essential to test the model in different environments and with different accessions. In this study, incorporating attention mechanisms such as SE, CBAM, and CEA led to significant improvements in cases with insufficient datasets, while their impact was less pronounced when the dataset was sufficiently large. Moreover, the composition of the dataset clearly affects the model performance. For instance, the predictions for the PFS (including EFS, MFS, LFS) were the most accurate, particularly for the LFS, while performance during IFS and TFS was poorer. This is likely due to the training dataset predominantly consisting of images from the PFS.

### Simple ANN for Basic Data

For relatively simple datasets, such as the flowering stage data in this study, a simple artificial neural network (ANN) suffices for classification tasks. After designing and comparing different network architectures in this study, it was found that increasing the complexity of the model does not lead to improvements in performance.

### Consideration of agronomic characteristics in quantifying different crop Traits

When quantifying agronomic traits in crops, it is essential to account for specific agronomic characteristics. For example, tea flower quantity is greatly influenced by light exposure, and there are substantial variations in flower quantity across different tea plant of the same row. Thus, it is important to collect a sufficient number of images from various locations within the field. Additionally, tea accessions exhibit differences in morphology-ranging from small trees to shrubs

and the significant image disparities between pruned and naturally grown trees require models with high generalization and robustness.

### **Influence of plant size and weather on Tea Flower Quantity**

Flower quantity is strongly correlated with the size of the tea plant. To compare flower quantities across different accessions, it is important to ensure that the comparisons are made between plants of similar size and management practices. When evaluating traits across different crop accessions, the variability between individual tea plants is considerable. Previous studies often focused on individual plants, with  $R^2$  values computed for single plants. While this approach is more accurate for individual trees, it is difficult to represent the overall situation and can be skewed by extreme individuals. In this study, I directly sampled by plot unit and evaluated performance of the model. Additionally, tea flower quantity is influenced by weather conditions. Due to climatic differences between 2023 and 2024, the flowering dynamics of the same accession varied significantly and flowering period was generally later in 2024 than in 2023, as the extreme low temperatures in November and December 2023 were lower than those in November and December 2024. It is speculated that the relatively high temperatures in October to December 2024 caused the tea flowering period to arrive later. In the future, it would be valuable to combine tea flowering data with meteorological data to analyze the dynamics of tea plant flowering.

### **Comparison with previous tea flower studies**

Although previous tea flower studies constructed by manual survey involved fewer accessions and only surveyed a limited number of plants, the overall flower quantity and stage trends align with our findings. For instance, the flower quantity of accessions like MX and TGY was consistently high across different studies, and HJG displayed relatively high quantity.

Compared to other species, tea flowers have a relatively long and overlapping blooming duration. Previous studies have shown that the flowering period of tea accessions from the Southern Yangtze tea region (e.g., Longjing accession) begins earlier, while the flowering period of tea accessions from the Southwest tea region (e.g., Yunnan large-leaf tea) starts later. Accessions from the South China tea region (e.g., Fuding Dabaicha) have flowering periods that fall in between these two extremes. In this study, the flowering period of tea accessions from the Southern Yangtze tea region begins earlier and tend to have longer flowering periods, while the accessions from the South China tea region (such as Fujian province) have later flowering periods.



## 5. CONCLUSIONS

This study proposes an effective framework for quantifying tea flowering, comprising the TflosYOLO model and TFSC model. Compared to traditional manual surveys and observations, this framework is more efficient and accurate. The TflosYOLO model demonstrates the ability to accurately detect tea flowers under various conditions, including different tea accessions, flowering stage, pruning practices, and lighting conditions. Its high robustness and generalization capability render it the only model currently suitable for both detecting tea flowers and predicting flower quantities, achieving state-of-the-art (SOTA) performance in this domain. TFSC model consistently demonstrates an accuracy exceeding 0.73 across different years, indicating its high generalizability. This framework facilitates dynamic observation and analysis of flower quantities and flowering stages.

There are differences in the flowering dynamics of various tea accessions. Accessions that are genetically related tend to exhibit more similar flower quantities and blooming periods. In particular, tea accessions from the Southern Yangtze tea region, which includes Hunan, Anhui, and Jiangxi provinces in this study, generally have earlier flowering periods and longer PFS. In contrast, tea accessions from Fujian, located in southern China, typically have later flowering periods. The flowering quantity and flowering period of the same accession can vary between different years due to changes in climate and management practices.

## ACKNOWLEDGMENTS

### **Author contributions:**

QM contributed to conceptualization, data collection, methodology, data analysis, writing-review & editing. JC contributed to conceptualization, writing-review & editing. MY contributed to review, Supervision. PY contributed to data collection. CM contributed to conceptualization.

**Funding:** This work was supported by the Major Project of Agricultural Science and Technology in Breeding of Tea Plant Variety in Zhejiang Province (2021C02067-1), the National Key Research and Development Program of China (2021YFD1200203), the Guangxi Key Research and Development Program (AB23026086), and the Fundamental Research Fund for Tea Research Institute of the Chinese Academy of Agricultural Sciences (1610212023003).

**Competing interests:** The authors declare that they have no competing interests.

**Data Availability:** The main code and some images of tea flowers used in this study are available at the GitHub repository: <https://github.com/sufie-mi/tea-flower-model>.

## References

1. Wang J, Shi Y, Zhang Y, Dong Z, Zeng T, Xi Y, Zhou S, Wang J. Effects of Flower Removal on the Yield and Biochemical Components of Spring Albino Tea. *Journal of Tea Communication*, 2022, 49(4): 464-471.
2. Tan X, Li H, Wang C, Tang D, Chen W, Tan L, Yang Y, Yang C, Tang Q. The removal of flower buds improves the yield and quality of tea shoots by mediating carbon and nitrogen metabolism in the source leaves. *Scientia Horticulturae*. 2024; 326:112735. doi:10.1016/j.scienta.2023.112735.
3. Paudel D, Boogaard H, de Wit A, Janssen S, Osinga S, Pylianidis C, Athanasiadis IN. Machine learning for large-scale crop yield forecasting. *Agricultural Systems*. 2021; 187:103016. doi:10.1016/j.agsy.2020.103016.
4. Chlingaryan A, Sukkarieh S, Whelan B. Machine learning approaches for crop yield prediction and nitrogen status estimation in precision agriculture: A review. *Computers and Electronics in Agriculture*. 2018; 151:61–69. doi:10.1016/j.compag.2018.05.012.
5. Liu S, Li X, Wu H, Xin B, Tang J, Petrie PR, Whitty M. A robust automated flower estimation system for grape vines. *Biosystems Engineering*. 2018; 172:110–123. doi:10.1016/j.biosystemseng.2018.05.009.
6. Song C, Zhang F, Li J, Xie J, Yang C, Zhou H, Zhang J. Detection of maize tassels for UAV remote sensing image with an improved YOLOX Model. *Journal of Integrative Agriculture*. 2023; 22(6):1671–1683. doi:10.1016/j.jia.2022.09.021.
7. Tu Y, Bian M, Wan Y, Fei T. Tea cultivar classification and biochemical parameter estimation from hyperspectral imagery obtained by UAV. *PeerJ*. 2018; 6:e4858. doi:10.7717/peerj.4858.
8. Chen S, Shen J, Fan K, Qian W, Gu H, Li Y, Zhang J, Han X, Wang Y, Ding Z. Hyperspectral machine-learning model for screening tea germplasm resources with drought tolerance. *Front. Plant Sci*. 2022; 13. doi:10.3389/fpls.2022.1048442.
9. Wang X (Annie), Tang J, Whitty M. DeepPhenology: Estimation of apple flower phenology distributions based on deep learning. *Computers and Electronics in Agriculture*. 2021; 185:106123. doi:10.1016/j.compag.2021.106123.
10. Xia X, Chai X, Li Z, Zhang N, Sun T. MTYOLOX: Multi-transformers-enabled YOLO for tree-level apple inflorescences detection and density mapping. *Computers and Electronics in Agriculture*. 2023; 209:107803. doi:10.1016/j.compag.2023.107803.
11. Liu X, An H, Cai W, Shao X. Deep learning in spectral analysis: Modeling and imaging. *TrAC Trends in Analytical Chemistry*. 2024; 172:117612. doi:10.1016/j.trac.2024.117612.
12. Li J, Zhang D, Yang F, Zhang Q, Pan S, Zhao X, Zhang Q, Han Y, Yang J, Wang K, Zhao C. TrG2P: A transfer learning-based tool integrating multi-trait data for accurate prediction of crop yield. *Plant Communications*. 2024; :100975. doi:10.1016/j.xplc.2024.100975.
13. Paudel D, de Wit A, Boogaard H, Marcos D, Osinga S, Athanasiadis IN. Interpretability of deep learning models for crop yield forecasting. *Computers and Electronics in Agriculture*. 2023; 206:107663. doi:10.1016/j.compag.2023.107663.
14. Wu J, Yang G, Yang H, Zhu Y, Li Z, Lei L, Zhao C. Extracting apple tree crown information from remote imagery using deep learning. *Computers and Electronics in Agriculture*. 2020; 174:105504. doi:10.1016/j.compag.2020.105504.

15. Li H, Mao Y, Shi H, Fan K, Sun L, Zaman S, Shen J, Li X, Bi C, Shen Y, Xu Y, Chen H, Ding Z, Wang Y. Establishment of deep learning model for the growth of tea cutting seedlings based on hyperspectral imaging technique. *Scientia Horticulturae*. 2024; 331:113106. doi:10.1016/j.scienta.2024.113106.
16. Sun Q, Chai X, Zeng Z, Zhou G, Sun T. Noise-tolerant RGB-D feature fusion network for outdoor fruit detection. *Computers and Electronics in Agriculture*. 2022; 198:107034. doi:10.1016/j.compag.2022.107034.
17. Wang A, Peng T, Cao H, Xu Y, Wei X, Cui B. TIA-YOLOv5: An improved YOLOv5 network for real-time detection of crop and weed in the field. *Front. Plant Sci*. 2022; 13. doi:10.3389/fpls.2022.1091655.
18. Rivera-Palacio JC, Bunn C, Rahn E, Little-Savage D, Schmidt PG, Ryo M. Geographic-Scale Coffee Cherry Counting with Smartphones and Deep Learning. *Plant Phenomics*. 2024; 6:0165. doi:10.34133/plantphenomics.0165.
19. Jocher G, Chaurasia A, Stoken A, Borovec J, NanoCode012, Kwon Y, Michael K, TaoXie, Fang J, imyhxy, Lorna, Zeng Y, Wong C, V A, Montes D, Wang Z, Fati C, Nadar J, Laughing, UnglvKitDe, Sonck V, tkianai, yxNONG, Skalski P, Hogan A, Nair D, Strobel M, Jain M. ultralytics/yolov5: v7.0 - YOLOv5 SOTA Realtime Instance Segmentation. 2022. doi:10.5281/zenodo.7347926.
20. Farjon G, Edan Y. AgroCounters—A repository for counting objects in images in the agricultural domain by using deep-learning algorithms: Framework and evaluation. *Computers and Electronics in Agriculture*. 2024; 222:108988. doi:10.1016/j.compag.2024.108988.
21. Guo Y, Fu YH, Chen S, Robin Bryant C, Li X, Senthilnath J, Sun H, Wang S, Wu Z, de Beurs K. Integrating spectral and textural information for identifying the tasseling date of summer maize using UAV based RGB images. *International Journal of Applied Earth Observation and Geoinformation*. 2021; 102:102435. doi:10.1016/j.jag.2021.102435.
22. Lyu M, Lu X, Shen Y, Tan Y, Wan L, Shu Q, He Y, He Y, Cen H. UAV time-series imagery with novel machine learning to estimate heading dates of rice accessions for breeding. *Agricultural and Forest Meteorology*. 2023; 341:109646. doi:10.1016/j.agrformet.2023.109646.
23. Yu X, Yin D, Nie C, Ming B, Xu H, Liu Y, Bai Y, Shao M, Cheng M, Liu Y, Liu S, Wang Z, Wang S, Shi L, Jin X. Maize tassel area dynamic monitoring based on near-ground and UAV RGB images by U-Net model. *Computers and Electronics in Agriculture*. 2022; 203:107477. doi:10.1016/j.compag.2022.107477.
24. Lin J, Li J, Ma Z, Li C, Huang G, Lu H. A Framework for Single-Panicle Litchi Flower Counting by Regression with Multitask Learning. *Plant Phenomics*. 6:0172. doi:10.34133/plantphenomics.0172.
25. Xia Y, Lei X, Qi Y, Xu T, Yuan Q, Pan J, Jiang S, Lyu X. Detection of pear inflorescence based on improved Ghost-YOLOv5s-BiFPN algorithm. *Smart Agriculture*, 2022, 4(3): 108119.
26. Sun K, Wang X, Liu S, Liu C. Apple, peach, and pear flower detection using semantic segmentation network and shape constraint level set. *Computers and Electronics in Agriculture*. 2021; 185:106150. doi:10.1016/j.compag.2021.106150.
27. Bhattarai U, Karkee M. A weakly-supervised approach for flower/fruit counting in apple orchards. *Computers in Industry*. 2022; 138:103635. doi:10.1016/j.compind.2022.103635.
28. Lin P, Lee WS, Chen YM, Peres N, Fraisse C. A deep-level region-based visual representation architecture for detecting strawberry flowers in an outdoor field. *Precision Agriculture*. 2020; 21(2):387–402. doi:10.1007/s11119-019-09673-7.
29. Bai B, Wang J, Li J, Yu L, Wen J, Han Y. T-YOLO: a lightweight and efficient detection model for nutrient bud in complex tea plantation environment. *J Sci Food Agric*. 2024; doi:10.1002/jsfa.13396.
30. Chen T, Li H, Chen J, Zeng Z, Han C, Wu W. Detection network for multi-size and multi-target tea bud leaves in the field of view via improved YOLOv7. *Computers and Electronics in Agriculture*. 2024; 218:108700. doi:10.1016/j.compag.2024.108700.

31. Wang S-M, Yu C-P, Ma J-H, Ouyang J-X, Zhao Z-M, Xuan Y-M, Fan D-M, Yu J-F, Wang X-C, Zheng X-Q. Tea yield estimation using UAV images and deep learning. *Industrial Crops and Products*. 2024; 212:118358. doi:10.1016/j.indcrop.2024.118358.
32. Wu Y, Chen J, He L, Gui J, Jia J. An RGB-D object detection model with high-generalization ability applied to tea harvesting robot for outdoor cross-variety tea shoots detection. *Journal of Field Robotics*. 2024; 41(4):1167–1186. doi:10.1002/rob.22318.
33. Zhang F, Sun H, Xie S, Dong C, Li Y, Xu Y, Zhang Z, Chen F. A tea bud segmentation, detection and picking point localization based on the MDY7-3PTB model. *Front. Plant Sci*. 2023; 14. doi:10.3389/fpls.2023.1199473.
34. Wang Z, Underwood J, Walsh KB. Machine vision assessment of mango orchard flowering. *Computers and Electronics in Agriculture*. 2018; 151:501–511. doi:10.1016/j.compag.2018.06.040.
35. Schindelin J, Arganda-Carreras I, Frise E, Kaynig V, Longair M, Pietzsch T, Preibisch S, Rueden C, Saalfeld S, Schmid B, Tinevez J-Y, White DJ, Hartenstein V, Eliceiri K, Tomancak P, Cardona A. Fiji: an open-source platform for biological-image analysis. *Nat Methods*. 2012; 9(7):676–682. doi:10.1038/nmeth.2019.
36. Tzutalin. LabelImg. Git code. 2015. <https://github.com/tzutalin/labelImg>.
37. Wang C-Y, Bochkovskiy A, Liao H-YM. YOLOv7: Trainable Bag-of-Freebies Sets New State-of-the-Art for Real-Time Object Detectors. In: 2023 IEEE/CVF Conference on Computer Vision and Pattern Recognition (CVPR). 2023. p. 7464–7475. doi:10.1109/CVPR52729.2023.00721.
38. Hu J, Shen L, Sun G. Squeeze-and-Excitation Networks [Internet]. In: 2018 IEEE/CVF Conference on Computer Vision and Pattern Recognition. 2018. p. 7132–7141. doi:10.1109/CVPR.2018.00745.
39. Guo M-H, Xu T-X, Liu J-J, Liu Z-N, Jiang P-T, Mu T-J, Zhang S-H, Martin RR, Cheng M-M, Hu S-M. Attention mechanisms in computer vision: A survey. *Comp. Visual Media*. 2022; 8(3):331–368. doi:10.1007/s41095-022-0271-y.
40. Ji Y, Chen Z, Cheng Q, Liu R, Li M, Yan X, Li G, Wang D, Fu L, Ma Y, Jin X, Zong X, Yang T. Estimation of plant height and yield based on UAV imagery in faba bean (*Vicia faba* L.). *Plant Methods*. 2022; 18(1):26. doi:10.1186/s13007-022-00861-7.

## Supplementary data

### Manual assessments

The tea plant flower quantity was classified into six levels, ranging from 0 to 5, with 0 indicating no flowers, 1 indicating almost no flowers, 2 representing a low overall flower density (with generally no more than 6 flowers on a single branch), 3 indicating a moderate overall flower density (with generally more than 6 flowers on a single branch), 4 representing a high overall flower density (with generally more than 10 flowers on a single branch and multiple flower buds at the same flowering point), and 5 representing the flower density higher than 4, where flowers are present in almost all positions on the tea plant row. (Fig. S2A). Observations of flowering conditions were performed across the entire tea row, and flower quantity levels were recorded for each tea accessions.

The flowering period of tea plants was categorized into stages: Initiation of Flowering Stage (IFS), Peak Flowering Stage (PFS), and Termination of Flowering Stage (TFS). The PFS was further divided into Early Peak Flowering Stage (EFS), Mid Peak Flowering Stage (MFS), and Late Peak Flowering Stage (LFS). Tea flowers were classified into three categories: buds, blooming flowers (B flower), and withered flowers (W flower). The determination of the tea flowering stage was based on the quantity and proportion of each flower type during different periods. For example, in this study the Initiation of Flowering Stage is defined as when over 80% of the flowers are buds, the Maximum Flowering Stage is characterized by more than 20% buds, over 40% blooming flowers, and less than 40% withered flowers, while the Termination of Flowering Stage is indicated by fewer than 10% buds and more than 40% withered flowers. A schematic diagram of the flowering stage classification is provided below. A schematic diagram of the flowering stage classification is provided in Fig. S2B.

### **The actual area of images calculated using Fiji**

We collect several images with a scale every time we capture images, the side length of the black square is 1 cm, as shown in Fig. S1. The black square was used as scale and then calculate the actual area corresponding to the regions in the image by Fiji. After calculating the actual area of ten images, obtain the average value  $-3690.33 \text{ cm}^2$ ,  $69.26\text{cm} \times 53.28\text{cm}$ .



Fig. S1. Calculate the actual area based on the scale by Fiji.



Fig. S2. Manual assessments of flower quantity and flowering stages. (A) tea flower quantity. (B) tea flower stage.

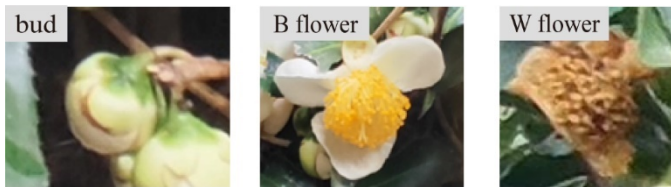


Fig. S3. Three categories of tea flower.

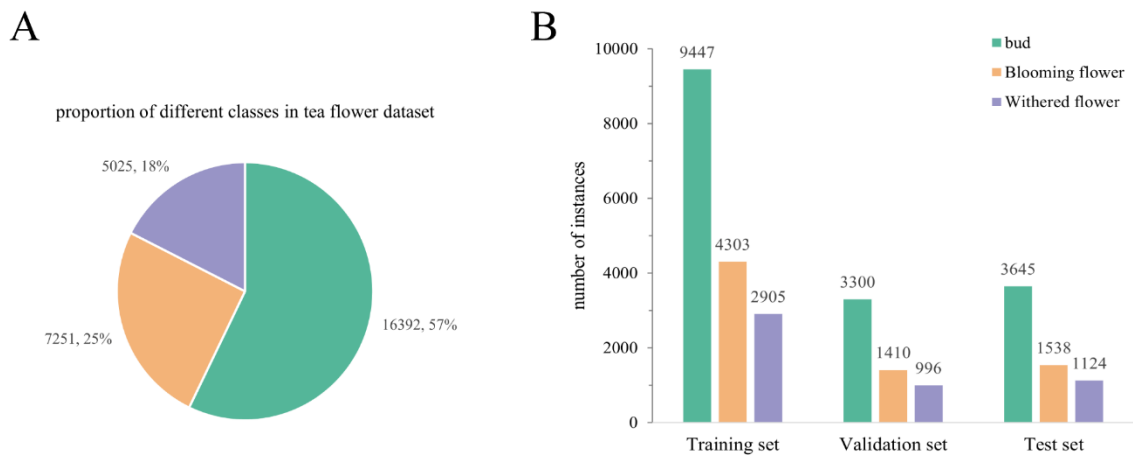


Fig. S4. Dataset analysis for tea flower detection model. (A) The proportion of buds, blooming flowers, and withered flowers within tea flower dataset (including training, validation, and testing dataset). (B) The quantity of buds, blooming flowers, and withered flowers within each dataset.

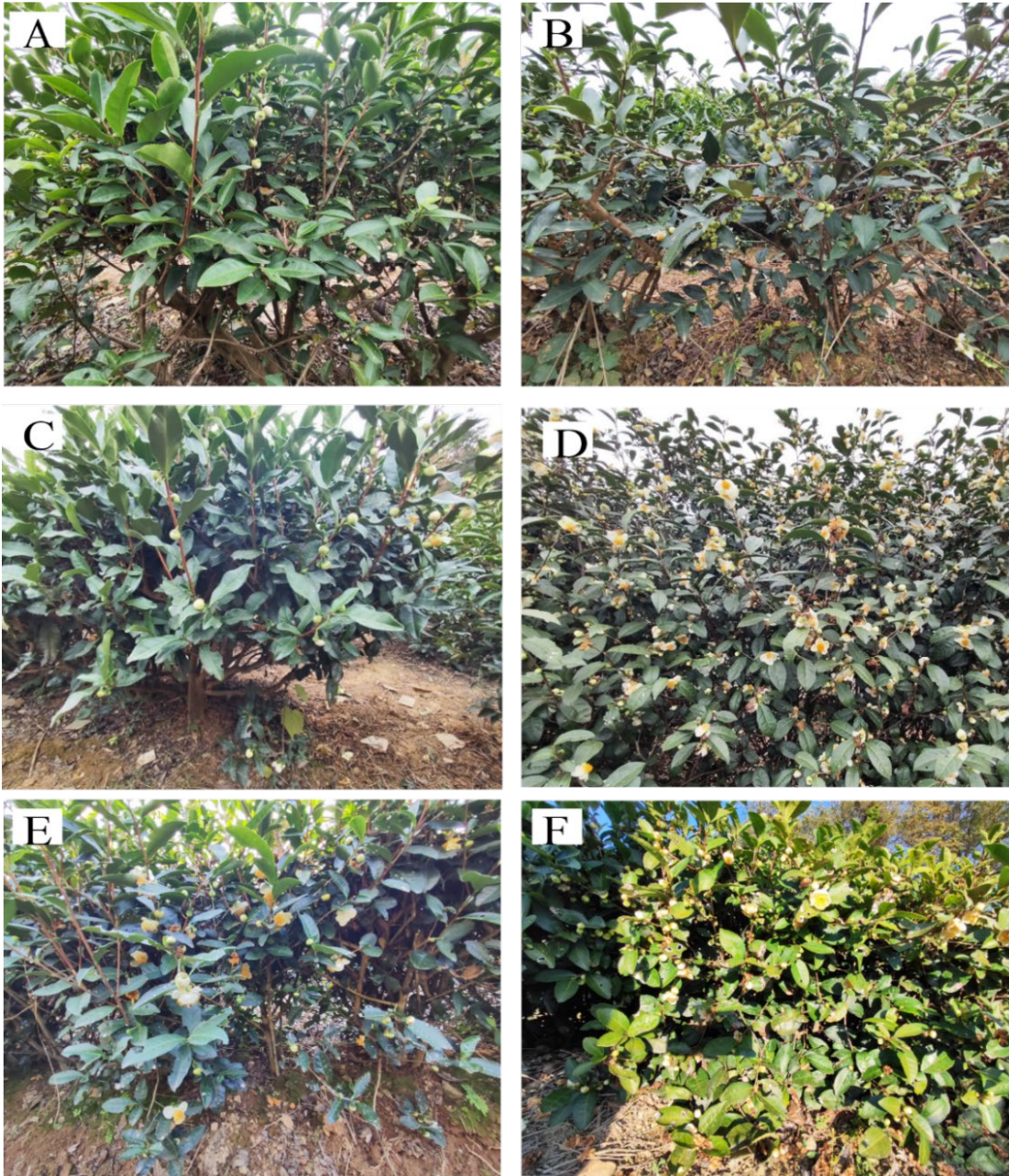


Fig. S5. The representative images of 34 additional test datasets. (A) accession(BHZ). (B) accession(TGY). (C) pruned tea plants. (D) unpruned tea plants. (E) tea plants under backlight. (F) tea plants under bright frontlight.



Fig. S6. TflosYOLO model detection performance on one image.

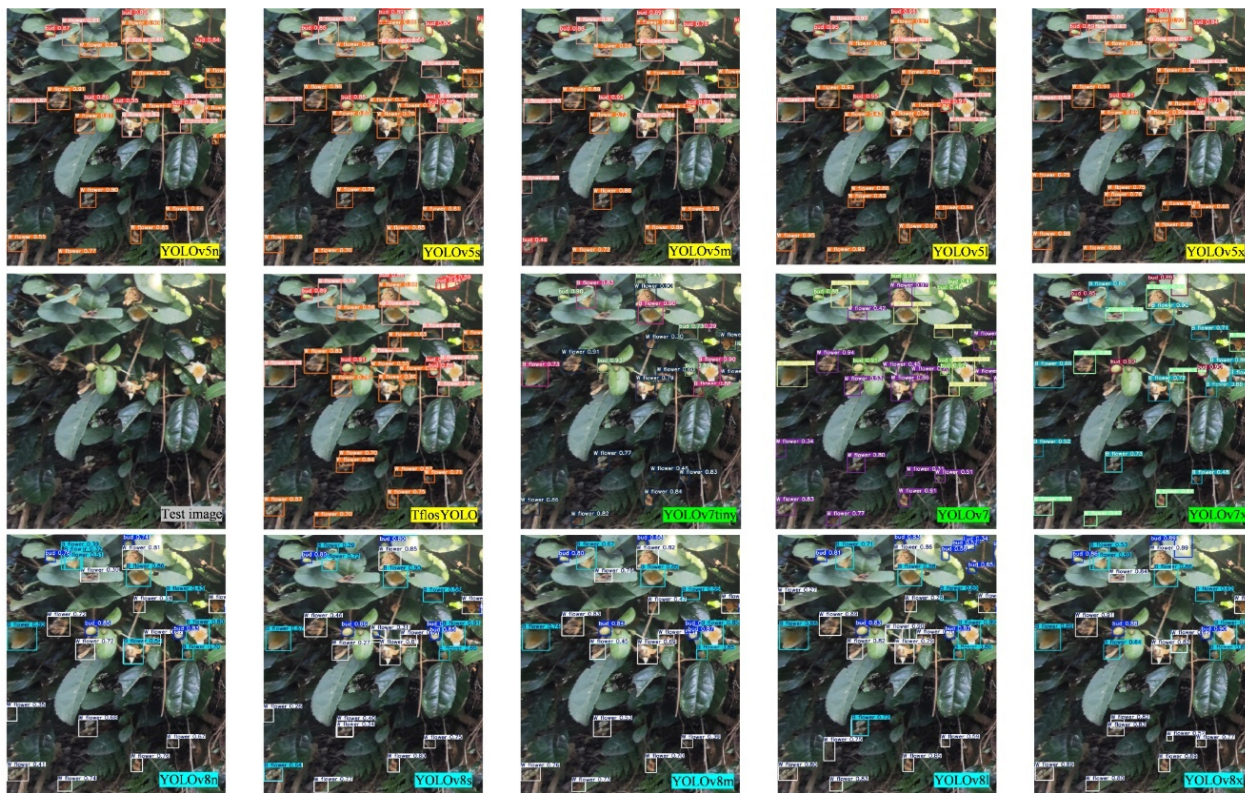


Fig. S7. Comparison of TflosYOLO with YOLOv5(n/s/m/l/x) & YOLOv7(tiny/yolov7/x) & YOLOv8(n/s/m/l/x) model under moderate lighting condition(backlight).



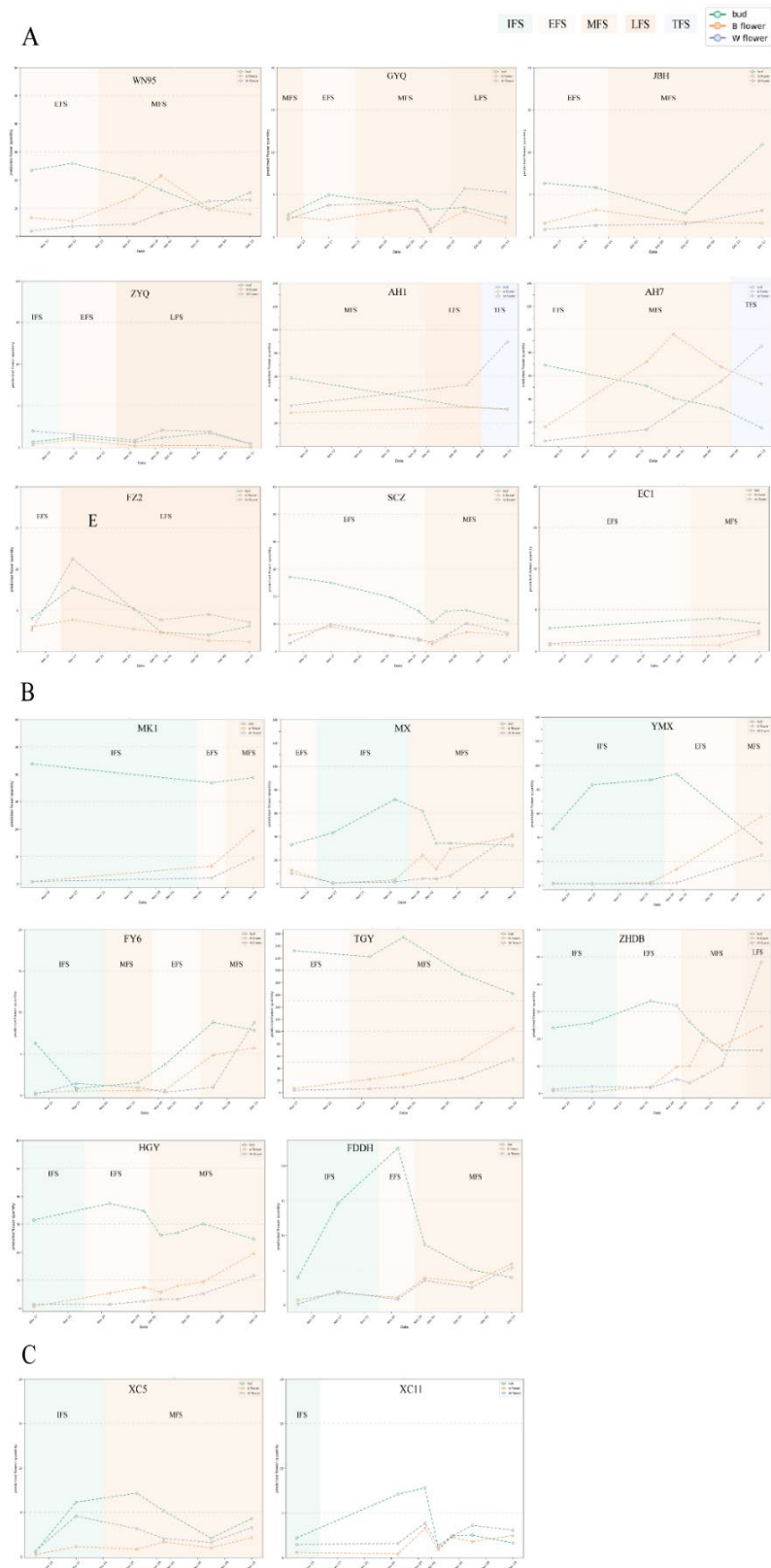


Fig. S8. The tea flowering dynamics and flowering stage information of 17 tea accessions in 2023. (A) The tea flowering dynamics of tea accessions from Anhui and Huan province (Southern Yangtze tea region); (B) The tea flowering dynamics of tea accessions from Fujian province (southern China tea region). (C) The accessions XC5 and XC11, based on their genetic lineage, were grouped in Jiangsu and Yunnan respectively.

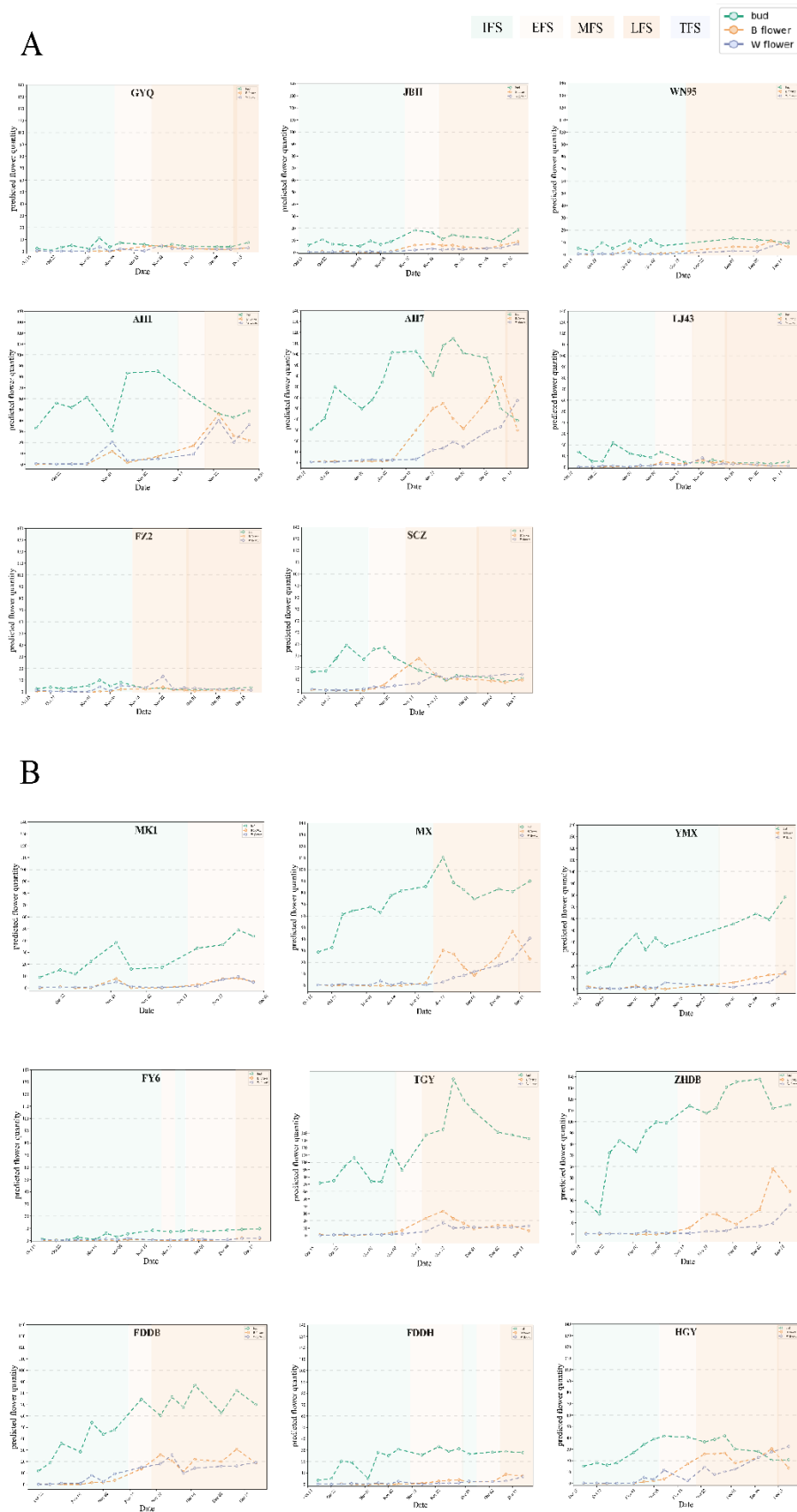


Fig. S9. The tea flowering dynamics of 17 tea accessions in 2024. (A) The tea flowering dynamics of tea accessions from Anhui, Zhejiang and Huan province; (B) The tea flowering dynamics of tea accessions from Fujian province.

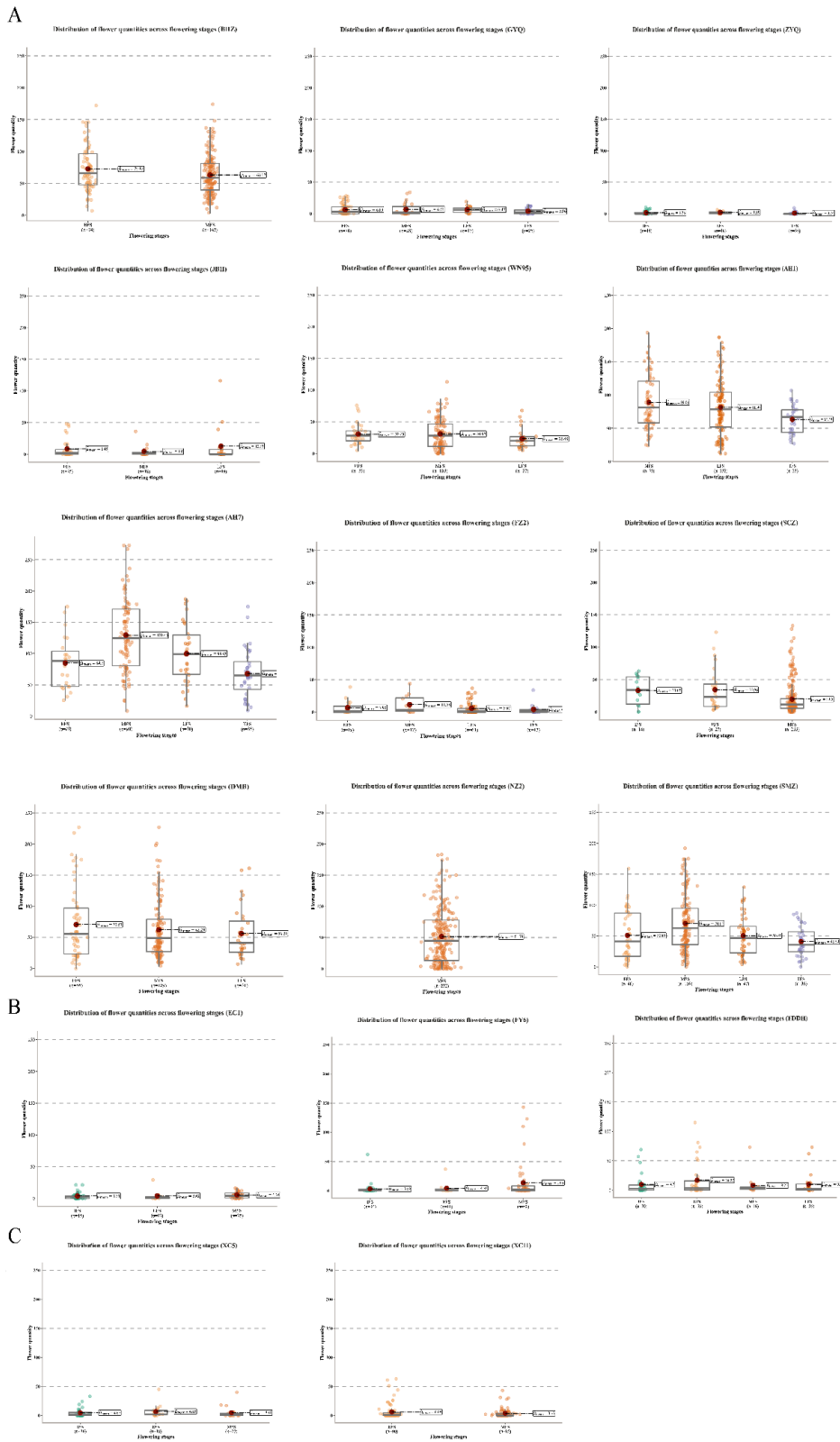


Fig. S10. Flower quantity data for each flowering stage (IFS, EFS, MFS, LFS, TFS) across accessions in 2023. (A) The tea flowering quantity of tea accessions from Anhui, Hunan and Jiangxi province (Southern Yangtze tea region); (B) The tea flowering quantity of tea accessions from Fujian province (southern China tea region). (C) The accessions XC5 and XC11, based on their genetic lineage, were grouped in Jiangsu and Yunnan, respectively.

Table S1. tea accessions information (not include in Table 1)

<b>accessions</b>	<b>abbreviation</b>
Fuding Dabaicha	FDDB
Longjing 43	LJ43
Anhui 3	AH3

Table S2. The amount of images for 34 additional test datasets

<b>additional test datasets</b>	<b>abbreviation</b>	<b>images</b>
Wannong95	WN95	40
Zhuyeqi	ZYQ	29
Gaoyaqi	GYQ	40
Baihaozao	BHZ	40
Jianbohuang	JBH	40
Anhui 1	AH1	40
Anhui7	AH7	40
Fuzao 2	FZ2	39
Shuchazao	SCZ	40
Damianbai	DMB	40
Ningzhou2	NZ2	40
Shangmeizhou	SMZ	40
Xicha 5	XC5	40
Echa 1	EC1	40
Fuding Dahaocha	FDDH	40
Fu'an Dabaicha	FADB	40
Zhenghe Dabaicha	ZHDB	40
Fuyun 6	FY6	40
Tie guanyin	TGY	40
Huang guanyin	HGY	40
Huang jingui	HJG	40
Huangqi	HQ	40
Mingke 1	MK1	40
Maoxie	MX	40
Yuemingxiang	YMX	40
Xicha 11	XC11	40
Initiation of Flowering Stage	IFS	111
Early Peak Flowering Stage	EFS	172
Mid Peak Flowering Stage	MFS	175
Late Peak Flowering Stage	LFS	64

Termination of Flowering Stage	TFS	33
Backlight		104
Front light		104
Unpruned		105

Table S3. Confusion matrix.

		Actual class	
		1	0
Predicted class	1	True Positive (TP)	False Positive (FP)
	0	False Negative (FN)	True Negative (TN)

Table S4. Accuracy of the TflosYOLO model based on validation dataset.

class	Precision	Recall	F <sub>1</sub> -score	mAP50	mAP50-95	params/ M	Model_size /M	GFlops
<b>All class</b>	<b>0.792</b>	<b>0.727</b>	<b>0.758</b>	<b>0.808</b>	<b>0.523</b>	<b>15.8</b>	<b>30.4</b>	<b>34.9</b>
bud	0.841	0.794	0.817	0.874	0.585			
B flower	0.769	0.769	0.765	0.817	0.512			
W flower	0.765	0.626	0.689	0.733	0.473			

Table S5. Accuracy of the TflosYOLO model based on 34 test dataset.

Test datasets	Precision	Recall	mAP50
Whole	0.802	0.854	0.874
WN95	0.839	0.825	0.884
ZYQ	0.679	0.944	0.809
GYQ	0.797	0.832	0.863
BHZ	0.824	0.834	0.877
JBH	0.755	0.888	0.856
AH1	0.778	0.868	0.88
AH7	0.818	0.884	0.895
FZ2	0.749	0.862	0.855
SCZ	0.849	0.85	0.907
DMB	0.818	0.832	0.876
NZ2	0.83	0.878	0.893
SMZ	0.779	0.811	0.836
XC5	0.797	0.948	0.894

EC1	0.695	0.663	0.741
FDDH	0.902	0.902	0.949
FADB	0.783	0.852	0.857
ZHDB	0.856	0.821	0.881
FY6	0.657	0.89	0.791
TGY	0.86	0.857	0.905
HGY	0.754	0.814	0.84
HJG	0.812	0.711	0.796
HQ	0.899	0.812	0.889
MK1	0.889	0.71	0.813
MX	0.818	0.858	0.871
YMX	0.753	0.851	0.858
XC11	0.726	0.828	0.809
IFS	0.733	0.764	0.796
EFS	0.794	0.781	0.825
MFS	0.817	0.849	0.879
LFS	0.82	0.838	0.889
TFS	0.723	0.778	0.816
Front light	0.763	0.748	0.804
Back light	0.854	0.891	0.914
Unpruned	0.801	0.839	0.863

---

Table S6. Accuracy of the TflosYOLO model based on AH7 test dataset.

class	Precision	Recall	mAP50
<b>All class</b>	<b>0.818</b>	<b>0.884</b>	<b>0.895</b>
bud	0.818	0.912	0.91
B flower	0.838	0.911	0.921
W flower	0.799	0.828	0.854

---

Table S7. Comparison of the TflorYOLO model accuracy among 5 flowering stages.

Flowering stage	class	Precision	Recall	mAP50
<b>IFS</b>	<b>all</b>	<b>0.733</b>	<b>0.764</b>	<b>0.796</b>
	bud	0.901	0.856	0.921
	B flower	0.602	0.714	0.751
	W flower	0.696	0.722	0.716
<b>EFS</b>	<b>all</b>	<b>0.794</b>	<b>0.781</b>	<b>0.825</b>
	bud	0.875	0.876	0.907
	B flower	0.833	0.807	0.866
	W flower	0.674	0.661	0.701
<b>MFS</b>	<b>all</b>	<b>0.817</b>	<b>0.849</b>	<b>0.879</b>
	bud	0.842	0.869	0.903
	B flower	0.864	0.873	0.913
	W flower	0.744	0.806	0.82
<b>LFS</b>	<b>all</b>	<b>0.82</b>	<b>0.838</b>	<b>0.889</b>
	bud	0.763	0.884	0.906
	B flower	0.848	0.832	0.893
	W flower	0.849	0.796	0.867
<b>TFS</b>	<b>all</b>	<b>0.723</b>	<b>0.778</b>	<b>0.816</b>
	bud	0.601	0.781	0.746
	B flower	0.722	0.811	0.855
	W flower	0.845	0.743	0.846

Table S8. Data samples of different accessions and Flowering Stage in time-series dataset across 2023 and 2024. (Data samples are shown as: 2023/2024).

Origin province		PFS					All stages
		IFS	EFS	MFS	LFS	TFS	
Hunan	WN95	0/92	33/31	103/42	27/0	0/0	163/165
	ZYQ	44/0	19/0	0/0	0/0	35/0	98/0
	GYQ	0/79	78/11	28/72	17/0	25/0	148/162
	BHZ	0/93	74/0	163/90	0/0	0/0	237/183
	JBH	0/86	35/45	18/44	19/0	0/0	72/175
Anhui	AH1	0/60	0/84	74/33	132/0	33/0	239/177
	AH3	0/88	0/12	0/78	0/0	0/0	0/178
	AH7	0/77	23/0	90/81	30/12	36/0	179/170

	FZ2	0/78	19/12	12/34	61/45	17/0	109/169
	SCZ	14/69	27/19	233/80	0/11	0/0	274/179
Jiangxi	DMB	0/87	56/24	129/70	31/0	0/0	216/181
	NZ2	0/78	0/11	232/87	0/0	0/0	232/176
	SMZ	0/93	46/0	156/93	47/0	36/0	285/186
Jiangsu	XC5	36/0	18/0	27/0	0/0	0/0	81/0
Fujian	EC1	45/0	13/0	35/0	0/0	0/0	93/0
	FDDH	30/86	35/54	16/22	26/0	0/0	107/0
	FADB	47/118	131/35	70/22	0/0	0/0	248/175
	ZHDB	48/91	145/13	165/77	42/0	0/0	400/0
	FY6	34/91	11/19	52/43	0/0	0/0	97/153
	TGY	0/66	24/17	102/90	0/0	0/0	126/173
	HGY	22/75	136/22	86/67	0/11	0/0	244/175
	HJG	155/128	48/12	36/34	0/0	0/0	239/174
	HQ	73/113	40/58	29/0	0/0	0/0	142/171
	MK1	146/105	64/93	0/0	0/0	0/0	210/198
	MX	0/102	180/23	183/55	0/0	0/0	363/180
	YMX	120/108	44/46	44/22	44/0	0/0	252/176
	FDDB	0/75	0/28	0/67	0/0	0/0	0/170
Yunnan	XC11	0/0	90/0	85/0	0/0	0/0	175/0
Zhejiang	LJ43	0/28	0/72	0/20	0/63	0/0	0/0
all		814/2211	1389/689	2168/1366	476/79	182/0	5029/4345

Table S9. the amount of buds, blooming flowers, and withered flowers at different flowering stages

Tea Flowering Stage	bud	Blooming flower	Withered flower
Initiation of Flowering Stage	29780	1207	1110
Early Peak Flowering Stage	54035	10787	5552
Mid Peak Flowering Stage	84205	48255	28180
Late Peak Flowering Stage	12189	13043	15100
Termination of Flowering Stage	2200	4006	8301
all	182409	77298	58243



Table S10. Comparison of flowering stage between different accessions based on model predictions and manual records.

Accession	Flowering Stage (Predicted by model)	Flowering Stage (manual)
WN95	early	early
BHZ	early	middle
GYQ	early	early
AH1	early	early
AH7	early	early
FZ2	early	early
DMB	early	early
NZ2	early	early
SMZ	early	early
TGY	early	early
ZYQ	middle	middle
JBH	middle	middle
SCZ	middle	middle
XC5	middle	middle
EC1	middle	middle
MX	middle	middle
FDDH	late	late
FADB	late	late
ZHDB	late	late
FY6	late	late
HGY	late	late
HJG	late	late
HQ	late	late
MK1	late	late
YMX	late	late